A homogenization-based theory for anisotropic beams with accurate through-section stress and strain prediction

Graeme J. Kennedy[a,1,*], Joaquim R.R.A. Martins[b,2]

[a] *University of Toronto Institute for Aerospace Studies, 4925 Dufferin Street, Toronto, Canada, M3H 5T6*

[b] *University of Michigan, Department of Aerospace Engineering, Ann Arbor, MI 48109*

Abstract

This paper presents a homogenization-based theory for three-dimensional anisotropic beams. The proposed beam theory uses a hierarchy of solutions to carefully-chosen beam problems that are referred to as the fundamental states. The stress and strain distribution in the beam is expressed as a linear combination of the fundamental state solutions and stress and strain residuals that capture the parts of the solution not accounted for by the fundamental states. This decomposition plays an important role in the homogenization process and provides a consistent method to reconstruct the stress and strain distribution in the beam in a post-processing calculation. A finite-element method is presented to calculate the fundamental state solutions. Results are presented demonstrating that the stress and strain reconstruction achieves accuracy comparable with full three-dimensional finite element computations, away from the ends of the beam. The computational cost of the proposed approach is three orders of magnitude less than the computational cost of full three-dimensional calculations for the cases presented here. For isotropic beams with symmetric cross-sections, the proposed theory takes the form of classical Timoshenko beam theory with Cowper's shear correction factor and additional load-dependent corrections. The proposed approach provides an extension of Timoshenko's beam theory that handles sections with anisotropic construction.

1. Introduction

Beam theories are developed based on a set of assumptions used to reduce the complex behavior of a slender, three-dimensional body to an equivalent one-dimensional problem. The usefulness of a beam theory is judged by its range of applicability, the accuracy of its results, and the effort required for analysis. In this paper we present a homogenization-based beam theory that takes a form similar to classical Timoshenko beam theory (Timoshenko, 1921, 1922), but is specifically designed for composite beams.

*Corresponding author

Email addresses: graeme.kennedy@utoronto.ca (Graeme J. Kennedy), jrram@umich.edu (Joaquim R.R.A. Martins)

[1] PhD Candidate

[2] Associate Professor

In our approach, we calibrate the stiffness properties, shear strain correction matrix, and load-dependent corrections within the theory based on a hierarchy of solutions that we call the *fundamental states*. The fundamental states are accurate sectional stress and strain solutions to a series of carefully-chosen, statically determinate beam problems. Since it is difficult to obtain exact solutions for the fundamental states for an arbitrary section, we formulate a finite-element solution technique to obtain approximate solutions.

This paper is structured as follows: In Section 2 we review some important contributions from the relevant literature. In Section 3 we outline the present theory. In Section 4 we present the finite-element based technique for the determination of the fundamental states. Finally, in Section 5 we present some results from the theory and present comparisons with full three-dimensional approximate solutions obtained using the finite-element method.

2. Review of relevant contributions

In this section we present a review of various contributions that are most relevant to our proposed beam theory. A comprehensive review of all beam theories is not practical here due to the volume of literature that has been produced on the subject over several decades.

In two influential papers, Timoshenko (1921, 1922) developed a beam theory for isotropic beams based on a plane stress assumption. Timoshenko's theory takes into account shear deformation and includes both displacement and rotation variables. In addition, Timoshenko introduced a shear correction factor that modifies the relationship between the shear resultant and the shear strain at the mid-surface. The definition and value of the shear correction factor have been the subject of many papers, some of which are discussed below.

Later, Prescott (1942) derived the equations of vibration for thin rods using average through-thickness displacement and rotation variables. Like Timoshenko, Prescott introduced a shear correction factor to account for the difference between the average shear on a cross-section and the expected quadratic distribution of shear.

Cowper (1966), independently from Prescott, developed a reinterpretation of Timoshenko beam theory based on average through-thickness displacements and rotations. Using these variables and integrating the equilibrium equations through the thickness, Cowper developed an expression for the shear correction factor, which he evaluated using the exact solution to a shear-loaded cantilever beam excluding end effects. Cowper obtained values for the shear coefficient for beams with various cross-sections, but his approach was limited to symmetric sections loaded in the plane of symmetry. Mason and Herrmann (1968) later extended the work of Cowper to include isotropic beams with an arbitrary cross-section.

Stephen and Levinson (1979) developed a beam theory along the lines of Cowper's, but recognized that the variation in shear along the length of the beam would lead to a modification of the relationship between bending moment and rotation. Therefore, they introduced a new correction factor to account for this variation, and obtained its value based on solutions to a cantilever beam subject to a constant body force given by Love (1920).

More recently, Hutchinson (2001) introduced a new Timoshenko beam formulation and computed the shear correction factor for various cross-sections based on a compar-

ison with a tip-loaded cantilever beam. For a beam with a rectangular cross-section, Hutchinson obtained a shear correction factor that depends on the Poisson ratio and the width to depth ratio. In a later discussion of this paper, Stephen (2001) showed that the shear correction factors he had obtained in earlier work (Stephen, 1980) were equivalent to Hutchinson.

Various authors have developed analysis techniques specifically for composite beams. Capturing shear deformation effects is, in general, more important for a composite beam than for a geometrically equivalent isotropic beam, due to the significantly lower ratio of the shear to extension modulus exhibited by composite materials. As a result, Timoshenko-type beam theories are often used to model composite beams. This type of approach is presented by many authors, such as Librescu and Song (2006) or Carrera et al. (2010b). Other authors have developed extensions to Cowper's approach. Dharmarajan and McCutchen (1973) extended Cowper's work to orthotropic beams, obtaining results for circular and rectangular cross-sections. Later, Bank (1987) and Bank and Melehan (1989) used Cowper's approach to develop expressions for the shear correction for thin-walled open and closed section orthotropic beams.

Numerous authors have developed refined beam and plate theories that are designed to better represent the through-thickness stress distribution behavior for both isotropic and composite plates and beams. For instance, Lo et al. (1977a,b) developed a higher-order plate theory for isotropic and laminated plates using a cubic through-thickness distribution of the in-plane displacements and quadratic out-of-plane displacements. Reddy (1987) developed a high-order plate theory for laminated plates based on a cubic through-thickness distribution of the in-plane displacements and obtained the equilibrium equations using the principle of virtual work. More recently, Carrera and Giunta (2010) developed a refined beam theory based on a hierarchical expansion of the through-section displacement distribution. This theory, which presents a unified framework, is more accurate than classical approaches (Carrera and Petrolo, 2011) and can be used for arbitrary sections composed of anisotropic materials. A finite-element approach using this refined beam theory has also been developed for both static (Carrera et al., 2010a) and free-vibration analysis (Carrera et al., 2011).

Although these higher-order theories are more accurate than classical Timoshenko beam theory, one drawback is their additional analytic and computational complexity. Furthermore, for laminated plates and beams, these theories predict a continuous through-thickness shear strain and discontinuous shear stress, whereas the expected distribution is discontinuous shear strain and continuous shear stress. Zig-zag theories address these through-thickness compatibility issues by employing a C^0, layer-wise continuous displacement. These types of theories were first developed by Lekhnitskii (1935). An extensive historical review of these theories was performed by Carrera (2003).

Many authors have used three-dimensional elasticity solutions as a way to improve the modeling capabilities of beam theories. Following the variational framework of Berdichevskii (1979), Cesnik and Hodges (1997) and Yu et al. (2002a) developed a variational asymptotic beam sectional analysis approach for the analysis of nonlinear orthotropic and anisotropic beams. In their approach, cross-sectional solutions containing all stress and strain components are used to calibrate the stiffness properties and reconstruct the stress distribution for a Timoshenko-like beam. The stiffness properties are recovered using an asymptotic expansion of the strain energy. Popescu and Hodges (2000) used this approach to examine the stiffness properties of anisotropic beams, focus-

ing in particular on the shear correction factor. Yu et al. (2002b) validated the approach of Cesnik and Hodges (1997) and Yu et al. (2002a) using full three-dimensional finite-element analysis.

Ladevéze and Simmonds (1998) and Ladevéze et al. (2002) presented an "exact" beam theory that uses three-dimensional Saint–Venant and Almansi–Michell solutions for the calibration of the stiffness properties of the beam and stress reconstruction. Using the framework set out by Ladevéze and Simmonds (1998) and Ladevéze et al. (2002), El Fatmi and Zenzri (2002) and El Fatmi and Zenzri (2004) developed a method for determining the Saint–Venant and Almansi–Michell solutions required by the "exact" beam theory using a computation only over the cross-section of the beam. El Fatmi (2007a,b) developed a beam theory based on non-uniform warping of the cross-section, using the framework of Ladevéze and Simmonds (1998). Their theory incorporated the Saint–Venant and Almansi–Michell solutions obtained by El Fatmi and Zenzri (2002, 2004).

Dong et al. (2001), using the techniques presented by Ieşan (1986a,b), developed a technique to solve the Saint–Venant problem for a general anisotropic beam of arbitrary construction. Kosmatka et al. (2001) determined the sectional properties, including the stiffness and shear center location, based on the finite-element technique of Dong et al. (2001).

Other authors have also used full three-dimensional solutions within the context of a beam theory. Gruttmann and Wagner (2001), following the work of Mason and Herrmann (1968), performed a finite-element-based analysis of isotropic beams with arbitrary cross-sections. Dong et al. (2010) used a semi-analytical finite-element formulation to compare shear correction factors for general isotropic sections computed using the methods of Cowper (1966), Hutchinson (2001), Schramm et al. (1994) and Popescu and Hodges (2000).

In this paper we extend our earlier work (Kennedy et al., 2011), which focused on layered orthotropic beams limited by a plane stress assumption. Here we examine three-dimensional, anisotropic beams. This is not a straightforward extension of our earlier work (Kennedy et al., 2011), as the coupling between shear and torsion adds an additional level of complexity.

An important feature of the present theory is the use of the *fundamental states*. The fundamental states are obtained from solutions to certain statically determinate beam problems. We use the fundamental state solutions to construct a relationship between stress and strain moments, and to reconstruct the stress and strain solution in a post-processing step. The fundamental states are the axially invariant components of the Saint–Venant and Almansi–Michell solutions. The key components of our theory include:

- The use of normalized displacement moments as a representation of the displacement in the beam, as used by Prescott (1942) and Cowper (1966).
- The use of strain moments as a representation of the strain state in the beam, as presented in (Kennedy et al., 2011) for plane stress problems.
- The homogenization of the relationship between stress and strain moments as used by Guiamatsia (2010) for plates.
- The representation of the full stress and strain field by an expansion of the solution using the fundamental state solutions.

- The strain moment correction matrix that corrects the strain predicted from the displacement moments.
- The use of load-dependent strain and stress moment corrections that modify the relationship between stress and strain moments in the presence of externally applied loads, as derived for plane stress problems by Kennedy et al. (2011).

Hansen and Almeida (2001) and Hansen et al. (2005) developed a theory with these same ideas for laminated and sandwich beams, using a plane stress assumption. An extension of this theory to the analysis of plates was presented by Guiamatsia and Hansen (2004) and Guiamatsia (2010).

These features of the present theory allow us to address several issues commonly encountered in conventional beam theories. The proposed theory contains a self-consistent method to obtain the equivalent stiffness of the beam and any correction factors required. In addition, all results from the theory, including the predicted strain moments, can easily be compared with three-dimensional results. This is due to the fact that all components of the theory rely on an averaging process that is well-defined for a beam of any construction, which is not always the case with conventional beam theories. These properties, in addition to the relatively inexpensive cost of analysis, make the proposed theory a powerful technique for analysis and design.

3. The homogenization-based beam theory

We present the theoretical development of the homogenization-based beam theory in this section. We start with a description of the geometry of the beam under consideration. Next, we develop a kinematic description of the beam using averaged displacement and rotation-type variables, based on the work of Prescott (1942) and Cowper (1966). We then introduce the fundamental states and use the properties of these solutions to develop expressions for the homogenized stiffness, stress and strain moment correction matrices, and load-dependent corrections. We conclude with a discussion of the benefits of the present approach.

The geometry of the beam under consideration is illustrated in Figure 1. The beam is aligned with the x-axis and the geometry and construction of the cross-section do not vary along the length of the beam. In this paper, we are primarily interested in layered composite beams with arbitrarily oriented plies. This type of beam construction results in an anisotropic constitutive relationship that exhibits coupling amongst all stress and strain components. The constitutive equation is expressed as

$$\boldsymbol{\sigma}(x,y,z) = \boldsymbol{C}(y,z)\boldsymbol{\epsilon}(x,y,z), \tag{1}$$

where $\boldsymbol{\sigma}(x,y,z)$ and $\boldsymbol{\epsilon}(x,y,z)$ are the full states of stress and strain, and $\boldsymbol{C}(y,z)$ is the constitutive relationship.

The beam of length L is subject to distributed surface tractions applied in the plane perpendicular to the x-axis and is subject to axial forces, bending moments, shear forces and torques at its ends. Shearing tractions applied on the surface of the beam in the x direction are excluded from consideration.

The reference axis is located at the geometric centroid of the section and the coordinate axes are aligned with the principal axes of the section. As a result, the moments of

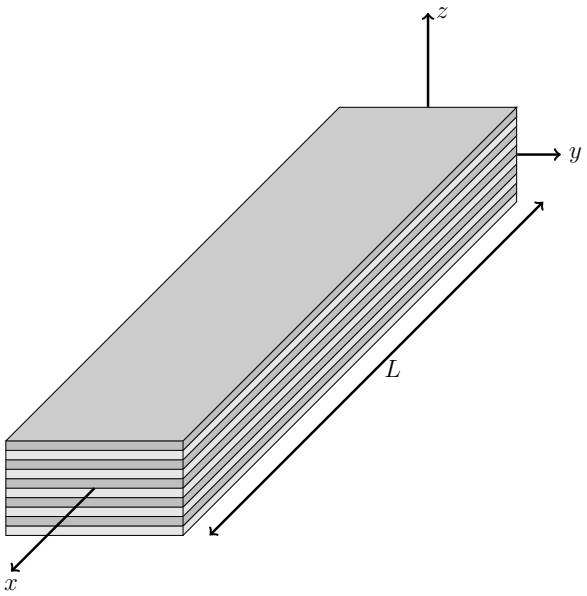

Figure 1: Geometry and reference coordinates for the beam composed of arbitrarily oriented composite layers.

area are defined as follows:

$$A = \int_\Omega d\Omega,$$
$$I_z = \int_\Omega z^2 \, d\Omega,$$
$$I_y = \int_\Omega y^2 \, d\Omega,$$
$$\int_\Omega y \, d\Omega = \int_\Omega z \, d\Omega = \int_\Omega yz \, d\Omega = 0.$$

The restriction to principal coordinate axes simplifies many of the expressions that are required below.

3.1. The displacement representation

Following the work of Prescott (1942) and Cowper (1966), the exact displacement field can be expressed in terms of an average representation of the displacement field and residual displacements. The residual displacements capture the part of the displacement field that deviates from the average representation. This decomposition of the

displacement field is expressed as

$$\boldsymbol{u}(x,y,z) = \begin{bmatrix} u(x,y,z) \\ v(x,y,z) \\ w(x,y,z) \end{bmatrix} = \begin{bmatrix} u_0(x) + zu_z(x) + yu_y(x) + \tilde{u}(x,y,z) \\ v_0(x) - z\theta(x) + \tilde{v}(x,y,z) \\ w_0(x) + y\theta(x) + \tilde{w}(x,y,z) \end{bmatrix}, \tag{2}$$

where $\boldsymbol{u}(x,y,z)$, and $\tilde{\boldsymbol{u}}(x,y,z) = \begin{bmatrix} \tilde{u} & \tilde{v} & \tilde{w} \end{bmatrix}^T$ are the displacements and residual displacements, respectively. The x-component of the residual displacement $\tilde{u}(x,y,z)$ represents the warping of the section in the axial direction. For convenience, we collect the variables, u_0, v_0, θ, u_z and u_y in a vector $\boldsymbol{u}_0(x)$, defined as follows:

$$\begin{aligned} \boldsymbol{u}_0(x) &= \begin{bmatrix} u_0 & v_0 & w_0 & \theta & u_z & u_y \end{bmatrix}^T \\ &= \int_\Omega \begin{bmatrix} \dfrac{u}{A} & \dfrac{v}{A} & \dfrac{w}{A} & \dfrac{(yw - zv)}{I_y + I_z} & \dfrac{zu}{I_z} & \dfrac{yu}{I_y} \end{bmatrix}^T d\Omega \\ &= \mathcal{L}_0 \boldsymbol{u}(x,y,z). \end{aligned} \tag{3}$$

Here, u_0, v_0, and w_0 are average displacements in the x, y and z directions. The terms u_z, u_y and θ are normalized first-order displacement moments about the z, y and x directions, respectively. Note that u_z, u_y and θ represent rotation-type variables, but are not equal to the average rotations of the section. We refer to the vector of variables $\boldsymbol{u}_0(x)$ as the normalized displacement moments, since these variables represent zeroth and first-order normalized moments of the displacement field $\boldsymbol{u}(x,y,z)$. In Equation (3), we have also introduced an operator $\mathcal{L}_0$ that takes the full three-dimensional displacement field, $\boldsymbol{u}(x,y,z)$, and returns the normalized moments of displacement. Note that the action of this operator removes the y-z dependence of the displacement field.

At this point it should be emphasized that the displacement field decomposition (2) ensures that the normalized displacement moments of the residual displacement field are identically zero, i.e.,

$$\mathcal{L}_0 \tilde{\boldsymbol{u}}(x,y,z) = 0.$$

This property of the residual displacement field will be required later to simplify expressions for the strain moments.

The strain produced by the displacements (2) is:

$$\boldsymbol{\epsilon}(x,y,z) = \begin{bmatrix} \epsilon_x \\ \epsilon_y \\ \epsilon_z \\ \gamma_{yz} \\ \gamma_{xz} \\ \gamma_{xy} \end{bmatrix} = \begin{bmatrix} u_{0,x} + yu_{y,x} + zu_{z,z} + \tilde{u}_{,x} \\ \tilde{v}_{,y} \\ \tilde{w}_{,z} \\ \tilde{v}_{,z} + \tilde{w}_{,y} \\ u_z + w_{0,x} + y\theta_{,x} + \tilde{u}_{,z} + \tilde{w}_{,x} \\ u_y + v_{0,x} - z\theta_{,x} + \tilde{u}_{,y} + \tilde{v}_{,x} \end{bmatrix}, \tag{4}$$

where the comma convention has been used to denote differentiation. Note that the exact pointwise strain distribution requires knowledge of the residual displacements $\tilde{\boldsymbol{u}}(x,y,z)$.

Instead of using the pointwise strain directly in our theory, we choose to use moments of the strain distribution. This choice has the advantage that the strain moments are defined regardless of the through-thickness behavior of the pointwise strain, even when certain pointwise strain components are discontinuous at material interfaces. It is im-

portant to recognize that these interfaces are always parallel to the x direction. As a result, differentiation with respect to x can commute with integration across the section in the regular manner.

The strain moments are defined as follows:

$$\begin{aligned}\boldsymbol{e}(x) &= \left[\begin{array}{cccccc} e_x & \kappa_z & \kappa_y & e_t & e_{xz} & e_{xy} \end{array}\right]^T \\ &= \int_\Omega \left[\begin{array}{ccccccc} \epsilon_x & z\epsilon_x & y\epsilon_x & (y\gamma_{xz} - z\gamma_{xy}) & \gamma_{xz} & \gamma_{xy} \end{array}\right]^T d\Omega \\ &= \mathcal{L}_s \boldsymbol{\epsilon}(x,y,z).\end{aligned} \tag{5}$$

Here we have introduced another operator $\mathcal{L}_s$ that takes the full strain field $\boldsymbol{\epsilon}(x,y,z)$ and returns the moments of strain $\boldsymbol{e}(x)$.

The next step in the development of the theory is to express the strain moments in terms of the displacement representation (2). Using the strain-displacement relationships (4), the definitions of the displacement moments (3), and the moments of area, the strain moments can be written as follows:

$$\boldsymbol{e}(x) = \left[\begin{array}{c} A u_{0,x} \\ I_z u_{z,x} \\ I_y u_{y,x} \\ (I_y + I_z)\,\theta_{,x} \\ A\,(u_z + w_{0,x}) \\ A\,(u_y + v_{0,x}) \end{array}\right] + \tilde{\boldsymbol{e}}(x) = \boldsymbol{A}\mathcal{L}_\epsilon \boldsymbol{u}_0(x) + \tilde{\boldsymbol{e}}(x), \tag{6}$$

where $\tilde{\boldsymbol{e}}(x)$ are the moments of the strain produced by the residual displacement. Here $\boldsymbol{A}$ is a diagonal matrix given by

$$\boldsymbol{A} = \mathrm{diag}\left\{A, I_z, I_y, (I_y + I_z), A, A\right\}.$$

The operator $\mathcal{L}_\epsilon$ takes the vector of average displacements and normalized displacement moments $\boldsymbol{u}_0(x)$, such that $\boldsymbol{A}\mathcal{L}_\epsilon \boldsymbol{u}_0$ produces the first term on the right hand side of Equation (6). Note that action of the operator $\mathcal{L}_\epsilon$ on the normalized displacements, $\mathcal{L}_\epsilon \boldsymbol{u}_0(x)$, produces terms that are identical in form to the center-line strain used in classical Timoshenko beam theory. However, the variables $\boldsymbol{u}_0(x)$ are interpreted here as normalized displacement moments taken from Equation (3), not as center-line displacements and rotations.

The term $\tilde{\boldsymbol{e}}(x)$ in the strain moment expression (6), is a function of the axial residual displacement $\tilde{u}(x,y,z)$ and is defined as follows:

$$\begin{aligned}\tilde{\boldsymbol{e}}(x) &= \int_\Omega \left[\begin{array}{c} \tilde{u}_{,x} \\ z\tilde{u}_{,x} \\ y\tilde{u}_{,x} \\ y\,(\tilde{u}_{,z} + \tilde{w}_{,x}) - z\,(\tilde{u}_{,y} + \tilde{v}_{,x}) \\ \tilde{u}_{,z} + \tilde{w}_{,x} \\ \tilde{u}_{,y} + \tilde{v}_{,x} \end{array}\right] d\Omega = \int_\Omega \left[\begin{array}{c} 0 \\ 0 \\ 0 \\ y\tilde{u}_{,z} - z\tilde{u}_{,y} \\ \tilde{u}_{,z} \\ \tilde{u}_{,y} \end{array}\right] d\Omega \\ &= \tilde{\mathcal{L}}\tilde{u}(x,y,z),\end{aligned} \tag{7}$$

where the relationship $\mathcal{L}_0\tilde{\boldsymbol{u}} = 0$ is used to simplify the expression on the right-hand side of the above equation. We have also introduced a linear operator $\tilde{\mathcal{L}}$ that takes the residual axial displacement $\tilde{u}(x, y, z)$ and returns the moments $\tilde{\boldsymbol{e}}(x)$.

The strain moments corresponding to torsion e_t and shear e_{xz} and e_{xy} involve terms from both the normalized displacement moments and the residual axial displacement, $\tilde{u}(x, y, z)$. These extra terms cannot be evaluated unless $\tilde{u}(x, y, z)$ is known. Our approach is to account for the effect of the residual displacements while formulating the theory in terms of the average displacement variables, $\boldsymbol{u}_0(x)$. The details of this approach are outlined in the following sections.

3.2. The equilibrium equations

The equilibrium equations are formulated based on the classical approach of integrating moments of the three-dimensional equilibrium equations over the cross-section of the beam. The axial, bending, torsion and shear resultants are defined as follows,

$$\begin{aligned}\boldsymbol{s}(x) &= \begin{bmatrix} N & M_z & M_y & T & Q_z & Q_y \end{bmatrix}^T \\ &= \int_\Omega \begin{bmatrix} \sigma_x & z\sigma_x & y\sigma_x & (y\sigma_{xz} - z\sigma_{xy}) & \sigma_{xz} & \sigma_{xy} \end{bmatrix}^T d\Omega \\ &= \mathcal{L}_s\boldsymbol{\sigma}(x, y, z).\end{aligned} \tag{8}$$

Here, $\mathcal{L}_s$ is the same operator that was introduced for the strain moments (5). We refer to the variables $\boldsymbol{s}(x)$ as the stress resultants (also known as stress moments). Integrating moments of the three-dimensional equilibrium equations over the section results in the following equilibrium equations:

$$\begin{bmatrix} N_{,x} \\ M_{y,x} - Q_z \\ M_{z,x} - Q_y \\ T_{,x} \\ Q_{y,x} \\ Q_{z,x} \end{bmatrix} + \begin{bmatrix} 0 \\ 0 \\ 0 \\ P_x \\ P_y \\ P_z \end{bmatrix} = 0. \tag{9}$$

The torque $P_x(x)$ and forces $P_y(x)$ and $P_z(x)$ are defined as follows:

$$\begin{aligned} P_x(x) &= \int_S yt_z - zt_y \, dS, \\ P_y(x) &= \int_S t_y \, dS, \\ P_z(x) &= \int_S t_z \, dS, \end{aligned} \tag{10}$$

where t_y and t_z are the y and z components of the surface traction. The integrals above are carried out over the boundary of the cross-section S.

3.3. The fundamental states

In this section we present a decomposition of the stress and strain distribution within the beam. This stress and strain decomposition is based on a linear combination of

axially-invariant stress and strain solutions that we call the *fundamental states*. The use of the fundamental states leads to a consistent method for deriving the constitutive relationship between the stress resultants and the strain moments. Furthermore, the fundamental states can be used to reconstruct the approximate stress and strain distribution in the beam in a post-processing step. Our representation of the solution is similar to the stress representation presented by Ladevéze and Simmonds (1998) and used by El Fatmi (2007a,b), however, unlike these authors, we also use an analogous representation of the strain solution that is later used to construct the homogenized stiffness relationship. In this section we describe the properties of the fundamental states and how they are used in the present theory.

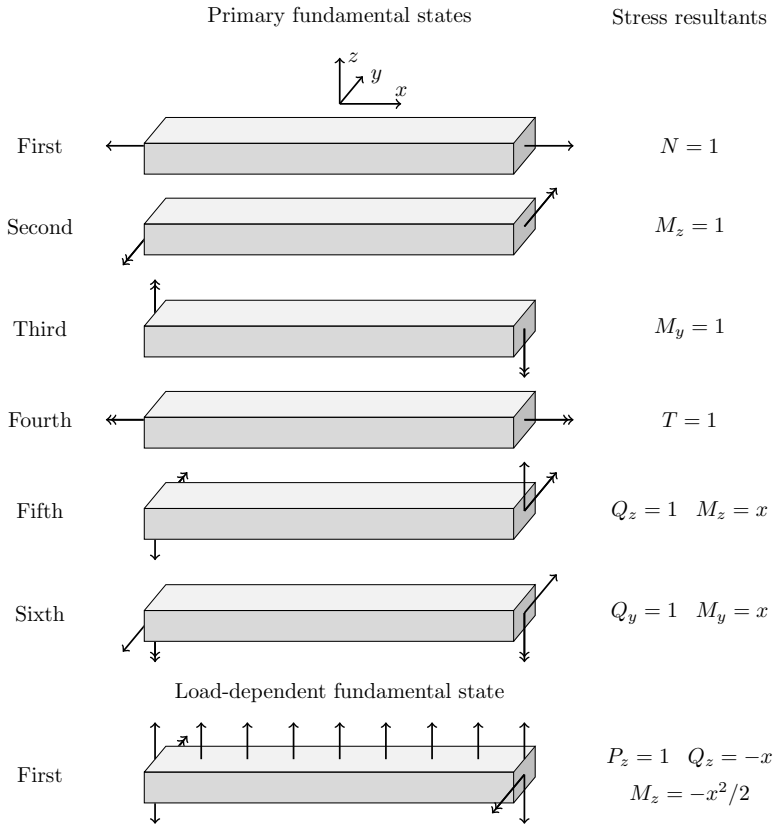

Figure 2: An illustration of the primary fundamental states and the distribution of the stress resultants. Forces are denoted by a single arrow and moments by a double arrow.

The fundamental states are the axially-invariant, or x-independent, stress and strain solutions. These solutions are obtained from specially-chosen, statically determinate beam problems. The loading conditions leading to the fundamental states are shown in Figure 2. These beam problems are sometimes referred to as the Saint–Venant prob-

lem (Ieşan, 1986a), for axial, bending, torsion, and shear loads, and the Almansi–Michell problem (Ieşan, 1986b), for a beam subject to a distributed surface load. The beam used to calculate the fundamental states has the same cross-section and construction as the beam under consideration, but must be long enough that the end effects do not alter the solution at the mid-plane of the beam. The fundamental states are extracted from these solutions by taking the distribution of stress and strain at the mid-plane of the beam. As a result, the fundamental state stress and strain distributions are solutions in the y-z and have no x-dependence.

We distinguish between two types of fundamental state solutions: primary fundamental states, which we label $\boldsymbol{\sigma}_F^{(k)}(y,z)$ and $\boldsymbol{\epsilon}_F^{(k)}(y,z)$, and load-dependent fundamental states, which we label $\boldsymbol{\sigma}_{LF}^{(k)}(y,z)$ and $\boldsymbol{\epsilon}_{LF}^{(k)}(y,z)$. The six primary fundamental states correspond to axial resultant, bending moments about the y and z axes, torsion, and shear in the z and y directions, respectively. The load-dependent fundamental states are associated with loads applied to the beam. The fundamental states are used here to form an approximation of the stress and strain field within the beam. To complete the stress and strain representation, we also introduce stress and strain residuals, $\tilde{\boldsymbol{\sigma}}(x,y,z)$ and $\tilde{\boldsymbol{\epsilon}}(x,y,z)$, that account for the discrepancy between the approximate stress and strain representation and the exact distribution.

Using these definitions, the stress and strain in the beam may be expressed as follows:

$$\boldsymbol{\sigma}(x,y,z) = \sum_{k=1}^{6} \boldsymbol{s}_k(x)\boldsymbol{\sigma}_F^{(k)}(y,z) + \sum_{k=1}^{N} P_k(x)\boldsymbol{\sigma}_{FL}^{(k)}(y,z) + \tilde{\boldsymbol{\sigma}}(x,y,z), \tag{11a}$$

$$\boldsymbol{\epsilon}(x,y,z) = \sum_{k=1}^{6} \boldsymbol{s}_k(x)\boldsymbol{\epsilon}_F^{(k)}(y,z) + \sum_{k=1}^{N} P_k(x)\boldsymbol{\epsilon}_{FL}^{(k)}(y,z) + \tilde{\boldsymbol{\epsilon}}(x,y,z). \tag{11b}$$

The magnitudes of the primary fundamental states are given by the components of the vector $\boldsymbol{s}(x)$ and represent axial force, bending moments, torsion, and shear resultants. Individual components of $\boldsymbol{s}(x)$ are written as $\boldsymbol{s}_k(x)$. The magnitudes of the load-dependent fundamental states $P_k(x)$ are known from the loading conditions. The fundamental state magnitudes link the stress and strain distribution.

For consistency between the stress resultants and the stress distribution, the primary fundamental states must satisfy the relationship,

$$\mathcal{L}_s\boldsymbol{\sigma}_F^{(k)}(y,z) = \boldsymbol{i}_k, \quad k = 1,\ldots,6, \tag{12}$$

where $\boldsymbol{i}_k$ is the k-th Cartesian basis vector. This relationship ensures that the stress resultants of the stress distribution (11a) are equal to $\boldsymbol{s}_k(x)$. Furthermore, the load-dependent fundamental states must satisfy

$$\mathcal{L}_s\boldsymbol{\sigma}_{FL}^{(k)}(y,z) = 0, \quad k = 1,\ldots,N. \tag{13}$$

The load-dependent fundamental states do not contribute to the stress resultants. In addition, the stress moments of the stress residuals must be zero, i.e.,

$$\mathcal{L}_s\tilde{\boldsymbol{\sigma}}(x,y,z) = 0.$$

An important benefit of the stress and strain distributions (11) is that they can capture all components of stress and strain. Typically, beam theories retain only a few components of the stress and strain and assume that the remaining components are negligible. These neglected components can sometimes be determined using a post-processing integration of the equilibrium equations through the thickness. For composite materials, however, it can be important to retain all components of stress and strain, since singularities can arise at ply interfaces and both strength and stiffness vary significantly between material directions (Pagano and Pipes, 1971).

3.4. The constitutive relationship

With these definitions, we are now prepared to derive the relationship between the stress resultants and the strain moments. To do so, we examine the moments of the strain field (11b). Using the moment operator $\mathcal{L}_s$, the strain moments of Equation (11b) become,

$$\boldsymbol{e}(x) = \sum_{k=1}^{6} \boldsymbol{s}_k(x)\mathcal{L}_s\boldsymbol{\epsilon}_F^{(k)}(y,z) + \sum_{k=1}^{N} P_k(x)\mathcal{L}_s\boldsymbol{\epsilon}_{FL}^{(k)}(y,z) + \mathcal{L}_s\tilde{\boldsymbol{\epsilon}}(x,y,z). \tag{14}$$

Note that the strain moments have contributions from all fundamental states and the strain residuals.

Next, we introduce a square flexibility matrix $\boldsymbol{E}$ whose k-th column contains the strain moments from the k-th primary fundamental state. The components of the matrix $\boldsymbol{E}$ are:

$$\boldsymbol{E}_{*k} = \mathcal{L}_s\boldsymbol{\epsilon}^{(k)}(y,z), \quad k = 1,\ldots,6, \tag{15}$$

where $\boldsymbol{E}_{*k}$ is the k-th column of the matrix $\boldsymbol{E}$. Note that the matrix $\boldsymbol{E}$ is constant for a given beam construction and is independent of x.

The contributions to the strain moments from the primary fundamental states are the product of the matrix $\boldsymbol{E}$ and the primary fundamental state magnitudes $\boldsymbol{s}(x)$. Re-arranging the strain moment relationship (14) and using the flexibility matrix $\boldsymbol{E}$ yields

$$\boldsymbol{E}\boldsymbol{s}(x) = \boldsymbol{e}(x) - \sum_{k=1}^{N} P_k(x)\mathcal{L}_s\boldsymbol{\epsilon}_{FL}^{(k)}(y,z) - \mathcal{L}_s\tilde{\boldsymbol{\epsilon}}(x,y,z). \tag{16}$$

The stiffness form of the constitutive relationship can be found by inverting the matrix of strain moments $\boldsymbol{D} = \boldsymbol{E}^{-1}$, to obtain

$$\boldsymbol{s}(x) = \boldsymbol{D}\left(\boldsymbol{e}(x) - \sum_{k=1}^{N} P_k(x)\mathcal{L}_s\boldsymbol{\epsilon}_{FL}^{(k)}(y,z) - \mathcal{L}_s\tilde{\boldsymbol{\epsilon}}(x,y,z)\right). \tag{17}$$

For a section composed of a single isotropic material the relationship between stress and strain moments simplifies to

$$\boldsymbol{D} = \operatorname{diag}\{E,E,E,G,G,G\}.$$

Equation (17) is exact in the sense that the stress moments can be determined exactly if the strain moments, load-dependent strain moments and strain residuals $\tilde{\boldsymbol{\epsilon}}(x,y,z)$ are

known. Unfortunately, evaluating the strain residuals $\tilde{\boldsymbol{\epsilon}}(x, y, z)$ requires a full three-dimensional solution of the equations of elasticity.

At this point, an assumption must be made about the contribution to the strain moments from the term $\mathcal{L}_s\tilde{\boldsymbol{\epsilon}}$. Since three-dimensional solutions are typically not available, we assume that the contribution from term $\mathcal{L}_s\tilde{\boldsymbol{\epsilon}}$ is small and can thus be neglected. This assumption introduces an error in the predicted strain moments, and as a result, also introduces an error in the predicted stress resultants. Typically, the magnitude of $\mathcal{L}_s\tilde{\epsilon}$ is highest near the ends of the beam where the solution must adjust to satisfy the end conditions. In situations where these disturbed regions require precise modeling, a beam theory is not appropriate. However, at a sufficient distance from the ends of the beam, the strain representation (11b) is accurate and thus $\mathcal{L}_s\tilde{\epsilon}$ should be small.

3.5. The stress and strain moment corrections

Next, we seek a relationship between strain moments and the normalized displacement moments. We initially limit the analysis to conditions where no external loads are applied to the beam. Starting from the stiffness form of the constitutive equations (17), and assuming that the strain residual moments are negligible $\mathcal{L}_s\tilde{\boldsymbol{\epsilon}} = 0$, the stress moments may be expressed in terms of the normalized displacement moments $\boldsymbol{u}_0(x)$ and the moments of the warping strain $\tilde{\boldsymbol{e}}(x)$ using Equation (6),

$$\boldsymbol{s}(x) = \boldsymbol{D}\left(\boldsymbol{A}\mathcal{L}_\epsilon\boldsymbol{u}_0(x) + \tilde{\boldsymbol{e}}(x)\right). \tag{18}$$

To proceed, an expression for $\tilde{\boldsymbol{e}}(x)$ must be obtained. Following the arguments presented by Cowper (1966), we argue that this term should be linearly dependent on the magnitudes of the primary fundamental states in regions sufficiently far removed from end effects or rapidly varying loads. We write this dependence as

$$\tilde{\boldsymbol{e}}(x) = \tilde{\boldsymbol{E}}\boldsymbol{s}(x) + \tilde{\boldsymbol{e}}_r, \tag{19}$$

where $\tilde{\boldsymbol{E}}$ is a flexibility matrix defined below. Here $\tilde{\boldsymbol{e}}_r$, is a warping residual term that accounts for the deviation of the warping moment in disturbed regions of the beam. We refer to $\tilde{\boldsymbol{e}}_r$ as the *strain correction error*.

Using the operator $\tilde{\mathcal{L}}$ from Equation (7), the matrix $\tilde{\boldsymbol{E}}$ can be written as

$$\tilde{\boldsymbol{E}}_{*k} = \tilde{\mathcal{L}}\tilde{u}_F^{(k)}(y, z), \quad k = 1, \ldots, 6, \tag{20}$$

where $\tilde{u}_F^{(k)}(y, z)$ is determined from the residual displacement of the k-th primary fundamental state. Note that due to the nature of the operator $\tilde{\mathcal{L}}$, the matrix $\tilde{\boldsymbol{E}}$ only has entries in the last three rows. All other entries in $\tilde{\boldsymbol{E}}$ are zero.

An expression for the stress resultants in terms of the normalized displacement moments can be obtained by using the simplified form of the constitutive relationship (18), and the moments of the strain due to warping (19), yielding

$$\boldsymbol{s}(x) = (\boldsymbol{E} - \tilde{\boldsymbol{E}})^{-1}\boldsymbol{A}\mathcal{L}_\epsilon\boldsymbol{u}_0(x) + (\boldsymbol{E} - \tilde{\boldsymbol{E}})^{-1}\tilde{\boldsymbol{e}}_r. \tag{21}$$

In the remainder of this section we assume that the strain correction error is negligible, i.e., $\tilde{\boldsymbol{e}}_r = 0$.

In order to isolate the effect of the terms $\tilde{\boldsymbol{E}}$ we define the strain moment correction matrix as follows:

$$\boldsymbol{C}_s = (\boldsymbol{I} - \tilde{\boldsymbol{E}}\boldsymbol{D})^{-1}, \tag{22}$$

such that Equation (21), with $\tilde{\boldsymbol{e}}_r = 0$, simplifies to

$$\boldsymbol{s}(x) = \boldsymbol{D}\boldsymbol{C}_s\boldsymbol{A}\mathcal{L}_\epsilon\boldsymbol{u}_0(x).$$

Here, the strain moment correction matrix (22) provides a correction to the strain moments predicted from the average displacements that accounts for $\tilde{\boldsymbol{e}}(x)$. Note that the strain moment correction matrix $\boldsymbol{C}_s$ has a specific structure. The first three rows of $\boldsymbol{C}_s$ are always equal to the identity matrix, while the last three rows may contain non-zeros in any location due to the definition of the matrix $\tilde{\boldsymbol{E}}$.

We also define a stress moment correction matrix as follows:

$$\boldsymbol{K}_s = (\boldsymbol{I} - \boldsymbol{D}\tilde{\boldsymbol{E}})^{-1}, \tag{23}$$

such that Equation (21), with $\tilde{\boldsymbol{e}}_r = 0$, simplifies to

$$\boldsymbol{s}(x) = \boldsymbol{K}_s\boldsymbol{D}\boldsymbol{A}\mathcal{L}_\epsilon\boldsymbol{u}_0(x).$$

The stress moment correction matrix (23) provides a correction to the stress moments that accounts for $\tilde{\boldsymbol{e}}(x)$. In general, the stress moment correction matrix $\boldsymbol{K}_s$ is fully populated.

In the case of a doubly symmetric, isotropic section, the stress and strain corrections matrices are diagonal and equal. In this case, $\boldsymbol{C}_s$ and $\boldsymbol{K}_s$ take the form

$$\boldsymbol{K}_s = \boldsymbol{C}_s = \mathrm{diag}\{1, 1, 1, k_t, k_{xz}, k_{xy}\},$$

where $k_t = J/(I_y + I_z)$ is the strain correction associated with torsion, and J is the torsional rigidity of the section. The shear strain correction factors k_{xz} and k_{xy} are identical to those obtained by Cowper (1966) and Mason and Herrmann (1968),

$$k_{xz} = \frac{2(1+\nu)I_z}{\frac{\nu}{2}(I_y - I_z) - \frac{A}{I_z}\int_\Omega z^2y^2 + z\chi_z\, d\Omega}$$
$$k_{xy} = \frac{2(1+\nu)I_y}{\frac{\nu}{2}(I_z - I_y) - \frac{A}{I_y}\int_\Omega z^2y^2 + y\chi_y\, d\Omega}$$

where χ_z and χ_y are classical Saint–Venant flexure functions (Love, 1920).

3.6. The load-dependent corrections

The constitutive relationship (21) derived above explicitly excluded the effect of externally applied loads. At this point, we derive load-dependent corrections that account for the effect of external loads. We start from the flexibility form of the constitutive equations (16), and neglect the moments of the strain residuals, assuming $\mathcal{L}_s\tilde{\boldsymbol{\epsilon}} = 0$. These

assumptions result in the following expression for the strain moments:

$$\boldsymbol{e}(x) = \boldsymbol{E}\boldsymbol{s}(x) + \sum_{k=1}^{N} P_k(x)\mathcal{L}_s\boldsymbol{\epsilon}_{FL}^{(k)}(y,z). \tag{24}$$

The next step is to obtain an expression for the strain moments $\boldsymbol{e}(x)$ as a function of the normalized displacement moments $\boldsymbol{u}_0(x)$. The externally applied loads produce additional moments of the warping strain. In an analogous manner to the primary fundamental state contributions, we assume that these moments of the warping strain are predicted by the load-dependent fundamental states and are proportional to the applied load. These assumptions result in the following expression:

$$\boldsymbol{e}(x) = \boldsymbol{A}\mathcal{L}_\epsilon\boldsymbol{u}_0(x) + \tilde{\boldsymbol{E}}\boldsymbol{s}(x) + \sum_{k=1}^{N} P_k(x)\tilde{\mathcal{L}}\tilde{u}_{FL}^{(k)}(y,z) + \tilde{\boldsymbol{e}}_r. \tag{25}$$

Here, $\tilde{u}_{FL}^{(k)}(y,z)$ denotes the warping function associated with the k-th load-dependent fundamental state and $\tilde{\boldsymbol{e}}_r$, is the strain correction error.

Again, assuming that $\tilde{\boldsymbol{e}}_r = 0$, the flexibility form of the constitutive equations (24) and the strain moment expression (25) can now be combined into a constitutive relationship that takes the following form:

$$\boldsymbol{s}(x) = (\boldsymbol{E} - \tilde{\boldsymbol{E}})^{-1}\boldsymbol{A}\mathcal{L}_\epsilon\boldsymbol{u}_0(x) + \sum_{k=1}^{N} P_k(x)\boldsymbol{s}_{FL}^{(k)}, \tag{26}$$

where the load-dependent stress moment corrections $\boldsymbol{s}_{FL}^{(k)}$ are defined as

$$\boldsymbol{s}_{FL}^{(k)} = (\boldsymbol{E} - \tilde{\boldsymbol{E}})^{-1}\left(\tilde{\mathcal{L}}\tilde{u}_{FL}^{(k)}(y,z) - \mathcal{L}_s\boldsymbol{\epsilon}_{FL}^{(k)}(y,z)\right). \tag{27}$$

In a similar fashion, it can be shown that the strain moments take the modified form

$$\boldsymbol{e}(x) = \boldsymbol{C}_s\boldsymbol{A}\mathcal{L}_\epsilon\boldsymbol{u}_0 + \sum_{k=1}^{N} P_k(x)\boldsymbol{e}_{FL}^{(k)}, \tag{28}$$

where the load-dependent strain moment corrections $\boldsymbol{e}_{FL}^{(k)}$ are defined as

$$\boldsymbol{e}_{FL}^{(k)} = \boldsymbol{C}_s\left(\tilde{\mathcal{L}}\tilde{u}_{FL}^{(k)}(y,z) - \mathcal{L}_s\boldsymbol{\epsilon}_{FL}^{(k)}(y,z)\right) + \mathcal{L}_s\boldsymbol{\epsilon}_{FL}^{(k)}(y,z). \tag{29}$$

The load-dependent stress moment corrections (27) and the load-dependent strain moment corrections (29) take into account the change in the relationship between the stress and strain moments and the normalized displacement moments as a result of externally applied loads. The externally applied loads do not directly produce stress moments; rather, these loads produce strain moments that must be taken into account in the constitutive relationship (26). The main assumptions required for the derivation of the constitutive expression are that the moments of the strain residuals, $\mathcal{L}_s\tilde{\boldsymbol{\epsilon}}$, and the

strain moment correction, $\tilde{\boldsymbol{e}}_r$, can be neglected. These assumptions are examined below in the numerical results section.

3.7. The asymmetry of the constitutive relationship

In general, the homogenized stiffness matrix $\boldsymbol{D}$, and the matrix product $\boldsymbol{D}\boldsymbol{C}_s\boldsymbol{A}$ are not symmetric. This is not a classical result and deserves attention. Linear constitutive relationships between pointwise stress and pointwise strain expressed in the form of Equation (1) are symmetric due to the existence of the strain energy density. However, the homogenized stiffness matrix $\boldsymbol{D}$ that relates the stress resultants to the strain moments cannot be derived from a strain energy density, since $\boldsymbol{D}$ relates integrated quantities. The integral of the pointwise strain energy density across the section cannot be related directly to the product of the integrals of stress and strain. As a result, $\boldsymbol{D}$ is not guaranteed to be symmetric. The matrix product $\boldsymbol{D}\boldsymbol{C}_s\boldsymbol{A}$ that relates the normalized displacement moments to the stress resultants is not symmetric for the same reason. Within the context of a finite-element implementation of the present beam theory, care must be taken to ensure that symmetry of the constitutive relationship is not assumed.

4. A finite-element method for the determination of the fundamental states

The fundamental states play an important role within the beam theory presented in the previous section. In principle, full three-dimensional solutions for each of the fundamental states are required before any analysis can be performed. It is possible to obtain some exact solutions to the fundamental states, as shown in Kennedy et al. (2011). However, we anticipate that it is only possible to obtain these exact solutions for a small set of geometries and beam constructions of interest. In order to solve more general problems, we have develop a finite-element method for the determination of the fundamental states for cross-sections of arbitrary geometry and construction.

It is possible to use conventional three-dimensional finite-elements to obtain the fundamental state solutions; however, this approach is computationally expensive due to the large, three-dimensional mesh requirements. Instead, we develop a technique that only requires computations in the plane of the section, eliminating the need to discretize the axial direction. This approach is possible due to the fact that the fundamental states are far-field solutions.

In developing the following finite-element method, we follow the work of Pipes and Pagano (1970), who used a semi-inverse approach to obtain the stress and strain distributions in a long beam subject to an axial load. We modify the form of the assumed displacement field proposed by Pipes and Pagano (1970), but retain the terms that account for the effects of axial force, bending, shear, and torsion. El Fatmi and Zenzri (2002) developed a similar technique to obtain the Saint–Venant and Almansi–Michell solutions based on the work of Ladevéze and Simmonds (1998). Dong et al. (2001) developed a finite-element solution technique for the Saint–Venant problem based on the work of Ieşan (1986a).

In the following section, all variables refer to a single fundamental state calculation. Relationships with the beam theory are described explicitly in Section 4.2. In this finite-element approach, we develop a displacement-based solution to the three-dimensional

equations of elasticity based on the following expansion of the displacement field in the axial direction:

$$
\begin{aligned}
u(x,y,z) &= \sum_{k=1}^{M} \left\{ \frac{x^k}{k!} \left(c_1^{(k)} + c_2^{(k)} z + c_3^{(k)} y \right) + \frac{x^{k-1}}{(k-1)!} U^{(k)}(y,z) \right\}, \\
v(x,y,z) &= \sum_{k=1}^{M} \left\{ \frac{x^k}{k!} \left(c_6^{(k)} - c_4^{(k)} z - c_3^{(k)} \frac{x}{k+1} \right) + \frac{x^{k-1}}{(k-1)!} V^{(k)}(y,z) \right\}, \\
w(x,y,z) &= \sum_{k=1}^{M} \left\{ \frac{x^k}{k!} \left(c_5^{(k)} + c_4^{(k)} y - c_2^{(k)} \frac{x}{k+1} \right) + \frac{x^{k-1}}{(k-1)!} W^{(k)}(y,z) \right\},
\end{aligned}
\tag{30}
$$

where the displacements $U^{(k)}(y,z)$, $V^{(k)}(y,z)$ and $W^{(k)}(y,z)$ are written as $\boldsymbol{U}^{(k)} = \begin{bmatrix} U^{(k)} & V^{(k)} & W^{(k)} \end{bmatrix}^T$, and are only functions of y and z. The terms $c_1^{(k)}$ through $c_6^{(k)}$ are constant across the section, and we refer to these as the invariants. It is convenient to collect $c_1^{(k)}$ through $c_6^{(k)}$ into a vector denoted $\boldsymbol{c}^{(k)} = \begin{bmatrix} c_1^{(k)} & \dots & c_6^{(k)} \end{bmatrix}^T$. The number of terms M, retained in the expansion is discussed in more detail below. Pipes and Pagano (1970) used a similar form of Equation (30) with $M = 1$ to determine the stresses in the vicinity of the free edge of a laminated composite beam subjected to an axial force. As we demonstrate below, the displacement field above can also be used to predict the stress and strain fields due to bending, torsion, shear, and applied loads.

When $M > 1$, the representation of the displacement field (30) is not unique. The invariants $c_1^{(k)}$ through $c_6^{(k)}$ define displacements that can be represented by $U^{(k+1)}$, $V^{(k+1)}$ and $W^{(k+1)}$. Furthermore, displacement boundary conditions must be imposed on the displacement field (30) to remove rigid body translation and rotation modes. In order to handle both of these issues, we impose the constraint

$$
\mathcal{L}_0 \boldsymbol{U}^{(k)}(y,z) = 0, \quad k = 1, \dots, M,
\tag{31}
$$

where $\mathcal{L}_0$ is the operator defined in (3). This constraint removes the rigid body translation and rotation modes for $k = 1$, and ensures that the displacements are uniquely defined for $k > 1$. A different method for imposing the boundary conditions could be applied, but we have found that Equation (31) simplifies later results in relation to the beam theory.

The strain produced by the displacement field (30) is most clearly expressed in the form,

$$
\boldsymbol{\epsilon}(x,y,z) = \sum_{k=1}^{M} \frac{x^{k-1}}{(k-1)!} \boldsymbol{\epsilon}^{(k)}(y,z),
\tag{32}
$$

where $\boldsymbol{\epsilon}^{(k)}(y,z)$ is a strain distribution in the y-z plane. In Equation (32), the coefficient

$\boldsymbol{\epsilon}^{(k)}$ is given by,

$$\boldsymbol{\epsilon}^{(k)}(y,z) = \begin{bmatrix} \epsilon_x^{(k)} \\ \epsilon_y^{(k)} \\ \epsilon_z^{(k)} \\ \gamma_{yz}^{(k)} \\ \gamma_{xz}^{(k)} \\ \gamma_{xy}^{(k)} \end{bmatrix} = \begin{bmatrix} c_1^{(k)} + c_2^{(k)} z + c_3^{(k)} y + U^{(k+1)} \\ V_{,y}^{(k)} \\ W_{,z}^{(k)} \\ V_{,z}^{(k)} + W_{,y}^{(k)} \\ c_5^{(k)} + c_4^{(k)} y + U_{,z}^{(k)} + W^{(k+1)} \\ c_6^{(k)} - c_4^{(k)} z + U_{,y}^{(k)} + V^{(k+1)} \end{bmatrix}, \quad k = 1, \ldots, M \tag{33}$$

with $U^{(M+1)} = V^{(M+1)} = W^{(M+1)} = 0$.

From the expression for the strain (32), it is clear that the stresses in the beam take the form

$$\boldsymbol{\sigma}(x,y,z) = \sum_{k=1}^{M} \frac{x^{k-1}}{(k-1)!} \boldsymbol{\sigma}^{(k)}(y,z). \tag{34}$$

Using this polynomial expansion for the stresses, the three-dimensional equilibrium equations are

$$\begin{aligned} \sigma_{xy,y}^{(k)} + \sigma_{xz,z}^{(k)} + \sigma_x^{(k+1)} &= 0, \\ \sigma_{y,y}^{(k)} + \sigma_{yz,z}^{(k)} + \sigma_{xy}^{(k+1)} &= 0, \quad k = 1, \ldots, M \\ \sigma_{yz,y}^{(k)} + \sigma_{z,z}^{(k)} + \sigma_{xz}^{(k+1)} &= 0, \end{aligned} \tag{35}$$

with $\boldsymbol{\sigma}^{(M+1)} = 0$. These are the same equations used by Love (1920) for the solution of a tip-loaded cantilever, and a beam subject to gravity load. Here, the next highest-order terms in the expansion appear as body forces for the current equilibrium equations. For the k-th coefficient, the body force is equivalent to

$$\boldsymbol{b}^{(k)} = \begin{bmatrix} \sigma_x^{(k+1)} \\ \sigma_{xy}^{(k+1)} \\ \sigma_{xz}^{(k+1)} \end{bmatrix}.$$

Using the expressions for the strain (33) in conjunction with the constitutive relationship (1) and the equilibrium equations (35) results in $3M$ partial differential equations for the displacements $\boldsymbol{U}^{(k)}$. The next task is to determine equations that can be used to determine the values of $\boldsymbol{c}^{(k)}$.

At this point, we use the property that the fundamental states are statically determinate. As a result, the moment equilibrium equations (9) can be integrated to obtain the stress moment distribution in the beam. Furthermore, we limit the load-dependent fundamental states to loads that are polynomials in the x direction. (Note that this restriction applies to the integrated pressure loads (10), but does not apply to the distribution of the tractions across the section.) With this additional assumption, it is always possible to obtain a solution for the stress moments in the form of a polynomial,

$$\boldsymbol{s}(x) = \sum_{k=1}^{M} \frac{x^{k-1}}{(k-1)!} \boldsymbol{s}_c^{(k)}, \tag{36}$$

where $\boldsymbol{s}_c^{(k)}$ is the k-th coefficient in the polynomial. Clearly, the value of M must be chosen such that $M-1$ is equal to the degree of the polynomial stress-moment distribution (36). The primary fundamental states corresponding to axial force, torsion and bending moments can be determined with $M=1$. The primary fundamental states corresponding to shear require a solution with $M=2$ corresponding to a linearly varying bending moment and constant shear. The load-dependent fundamental state corresponding to a distributed surface loads requires $M=3$, with a quadratically varying bending moment and linearly varying shear.

For the moments of the stress expansion (34) to match the coefficients of the stress moment polynomial (36), we impose the additional constraint,

$$\mathcal{L}_s \boldsymbol{\sigma}^{(k)}(y,z) = \boldsymbol{s}_c^{(k)}, \quad k=1,\ldots,M. \tag{37}$$

These constraints represent an additional $6M$ equations that are used to determine $\boldsymbol{c}^{(k)}$.

To summarize, there are $3M$, $\boldsymbol{U}^{(k)}(y,z)$ coefficients defined in the y-z plane, and an additional $6M$ constants $\boldsymbol{c}^{(k)}$ that are required in the displacement field (30). These variables can be determined from the $6M$ moment constraints (37) and the $3M$ equilibrium equations (35) used in conjunction with the strain expressions (33) and the constitutive relationship (1).

It is important to note that this system of equations can be solved in a sequential fashion. The coefficients of the highest order $k=M$, $\boldsymbol{U}^{(M)}$, and $\boldsymbol{c}^{(M)}$, are independent of the lower order coefficients $k<M$. The $k=M$ terms couple with the next terms, $k=M-1$, $\boldsymbol{U}^{(M-1)}$, and $\boldsymbol{c}^{(M-1)}$, through the equivalent body-force terms in the equilibrium equations (35). This sequential process continues until all the coefficients, $\boldsymbol{U}^{(k)}$, and $\boldsymbol{c}^{(k)}$, have been determined. This same solution technique was used by Love (1920) for isotropic beams.

4.1. Finite-element implementation

We use a straightforward finite-element implementation of the above equations. This implementation shares many similarities with the approach of Dong et al. (2001). Here we pose our problem in terms of the displacement of the beam under the action of a prescribed load. Dong et al. (2001) seeks a solution in two steps: first obtaining the distribution of the warping displacements for axial, bending, torsion, and shear, then obtaining the amplitudes of the Saint–Venant solution in a second calculation. Here we employ conventional isoparametric displacement-based elements with bi-cubic Lagrangian shape functions in the plane for the $3M$ displacement field components $\boldsymbol{U}^{(k)}(y,z)$, $k=1,\ldots,M$. We write the nodal displacements of $\boldsymbol{U}^{(k)}(y,z)$ in the vector $\boldsymbol{d}^{(k)}$. It can be shown that the constraints on the stress moments (37) arise naturally using the principle of stationary total potential energy. We impose the unconventional displacement boundary conditions (31) by adding Lagrange multipliers and employ a Gauss quadrature approximation of the constraint (31). The discrete form of the displacement constraint is written as

$$\boldsymbol{L}_0 \boldsymbol{d}^{(k)} = 0,$$

where $\boldsymbol{L}_0$ is the discrete analogue of $\mathcal{L}_0$. We denote the Lagrange multipliers associated with the displacement constraints as $\boldsymbol{\lambda}^{(k)}$.

The discrete approximation of the k-th coefficient of the strain expansion (33) is written as

$$\boldsymbol{\epsilon}^{(k)} = \boldsymbol{B}\boldsymbol{d}_e^{(k)} + \boldsymbol{B}_c\boldsymbol{c}^{(k)} + \boldsymbol{B}_u\boldsymbol{d}_e^{(k+1)},$$

where $\boldsymbol{B}$, $\boldsymbol{B}_c$ and $\boldsymbol{B}_u$ take the nodal k-th displacements, k-th invariants and $k+1$-th displacement and produce the pointwise strain. Here, the subscript e has been used to denote the element displacements from the vector $\boldsymbol{d}^{(k)}$. The matrices $\boldsymbol{B}$ and $\boldsymbol{B}_u$ are defined as follows:

$$\boldsymbol{B} = \begin{bmatrix} 0 & 0 & 0 & \dots \\ 0 & N_{1,y} & 0 & \dots \\ 0 & 0 & N_{1,z} & \dots \\ 0 & N_{1,z} & N_{1,y} & \dots \\ N_{1,z} & 0 & 0 & \dots \\ N_{1,y} & 0 & 0 & \dots \end{bmatrix}, \quad \boldsymbol{B}_u = \begin{bmatrix} N_1 & 0 & 0 & \dots \\ 0 & 0 & 0 & \dots \\ 0 & 0 & 0 & \dots \\ 0 & 0 & 0 & \dots \\ 0 & 0 & N_1 & \dots \\ 0 & N_1 & 0 & \dots \end{bmatrix},$$

where N_i are the shape functions, and the comma notation has been used for differentiation. The pattern in the matrices $\boldsymbol{B}$ and $\boldsymbol{B}_u$, repeats itself for each node. The matrix $\boldsymbol{B}_c$ is given by

$$\boldsymbol{B}_c = \begin{bmatrix} 1 & z & y & 0 & 0 & 0 \\ 0 & 0 & 0 & 0 & 0 & 0 \\ 0 & 0 & 0 & 0 & 0 & 0 \\ 0 & 0 & 0 & 0 & 0 & 0 \\ 0 & 0 & 0 & y & 1 & 0 \\ 0 & 0 & 0 & -z & 0 & 1 \end{bmatrix}.$$

For convenience, we introduce the element matrices in a block matrix form as follows:

$$\begin{bmatrix} \boldsymbol{K}_{dd}^e & & \\ \boldsymbol{K}_{cd}^e & \boldsymbol{K}_{cc}^e & \\ \boldsymbol{K}_{ud}^e & \boldsymbol{K}_{uc}^e & \boldsymbol{K}_{uu}^e \end{bmatrix} = \int_{\Omega_e} \begin{bmatrix} \boldsymbol{B}^T\boldsymbol{C}\boldsymbol{B} & & \\ \boldsymbol{B}_c^T\boldsymbol{C}\boldsymbol{B} & \boldsymbol{B}_c^T\boldsymbol{C}\boldsymbol{B}_c & \\ \boldsymbol{B}_u^T\boldsymbol{C}\boldsymbol{B} & \boldsymbol{B}_u^T\boldsymbol{C}\boldsymbol{B}_c & \boldsymbol{B}_u^T\boldsymbol{C}\boldsymbol{B}_u \end{bmatrix} d\Omega_e, \tag{38}$$

where Ω_e is the element domain. The element matrices are denoted with a superscript e. The superscript e is omitted for the assembled form of the matrix.

The assembled finite-element equations are:

$$\begin{bmatrix} \boldsymbol{K}_{dd} & \boldsymbol{K}_{cd}^T & \boldsymbol{L}_0^T \\ \boldsymbol{K}_{cd} & \boldsymbol{K}_{cc} & 0 \\ \boldsymbol{L}_0 & 0 & 0 \end{bmatrix} \begin{bmatrix} \boldsymbol{d}^{(k)} \\ \boldsymbol{c}^{(k)} \\ \boldsymbol{\lambda}^{(k)} \end{bmatrix} = \begin{bmatrix} \boldsymbol{f}^{(k)} \\ \boldsymbol{f}_c^{(k)} \\ 0 \end{bmatrix}. \tag{39}$$

Care must be exercised when solving equation (39), since the matrix $\boldsymbol{K}_{dd}$ is singular. This is due to the fact that no conventional Dirichlet boundary conditions are applied to $\boldsymbol{K}_{dd}$. However, the final row of the system of equations (39) imposes a constraint that removes this singularity.

The two terms on the right hand side of Equation (39) are

$$\begin{aligned} \boldsymbol{f}^{(k)} &= \boldsymbol{f}_s^{(k)} + \boldsymbol{f}_b^{(k)} - \boldsymbol{K}_{ud}^T\boldsymbol{d}^{(k+1)}, \\ \boldsymbol{f}_c^{(k)} &= \boldsymbol{s}_c^{(k)} - \boldsymbol{K}_{uc}^T\boldsymbol{d}^{(k+1)}, \end{aligned} \tag{40}$$

where terms with superscripts greater than M are zero. The term $\boldsymbol{f}_s$ is the surface traction contribution to the right hand side and $\boldsymbol{f}_c$ is the right hand side for the invariants. The force vector, $\boldsymbol{f}_b^{(k)}$, represents a body force associated with the $k+1$-th fundamental state, defined as follows:

$$\boldsymbol{f}_b^{(k)} = \boldsymbol{K}_{ud}\boldsymbol{d}^{(k+1)} + \boldsymbol{K}_{uc}\boldsymbol{c}^{(k+1)} + \boldsymbol{K}_{uu}\boldsymbol{d}^{(k+2)}.$$

Note that the left hand side of Equation (39) is the same for each coefficient k. Therefore, only the right hand sides (40) needs to be recomputed in each subsequent solution.

4.2. Relation to beam theory

In this section we outline the connection between the finite-element approach described above and the proposed beam theory.

The computations outlined above are performed for each fundamental state. First, the polynomial stress resultant coefficients from Equation (36) are determined. These polynomials are summarized for each of the fundamental states in Figure 2. Next, the unknowns $\boldsymbol{d}^{(k)}$ and $\boldsymbol{c}^{(k)}$, $k = 1 \ldots M$, are determined using Equation (39). The fundamental state stress and strain solutions are the lowest-order terms of the polynomial expressions for the stress in Equations (34) and (32), respectively. Therefore, the fundamental states are $\boldsymbol{\sigma}^{(1)(y,z)}$ and $\boldsymbol{\epsilon}^{(1)}(y,z)$ in the y-z plane.

With this definition, the strain moments of the fundamental state can be computed using

$$\boldsymbol{e} = \boldsymbol{L}_s\boldsymbol{\epsilon}^{(1)}(y,z), \tag{41}$$

where $\boldsymbol{L}_s$ is a discrete analogue of the operator $\mathcal{L}_s$ computed using Gaussian quadrature. The strain moments are required to compute the flexibility matrix $\boldsymbol{E}$ (15) and for components of the stress and strain moment corrections in Equations (27) and (29), respectively.

Another key quantity required for the beam theory is the axial warping $\tilde{u}(x,y,z)$. The x-independent component of axial warping is precisely $U^{(1)}(y,z)$ due to the imposition of the displacement moment constraint (31). The moments of the warping strain can be evaluated using:

$$\tilde{\boldsymbol{e}} = \tilde{\boldsymbol{L}}U^{(1)}(y,z), \tag{42}$$

where $\tilde{\boldsymbol{L}}$ is the discrete analogue of $\tilde{\mathcal{L}}$ and is computed using Gaussian quadrature. The terms $\tilde{\boldsymbol{e}}$ are required for computing the flexibility matrix $\tilde{\boldsymbol{E}}$ (20), and the stress and strain moment correction matrices $\boldsymbol{K}_s$ (23) and $\boldsymbol{C}_s$ (22), respectively.

5. Results

In this section we present results using the finite-element approach presented in Section 4, and demonstrate the modeling capabilities of the beam theory. This section is divided into three parts. In the first part we compare the present beam theory results to results obtained by Cowper (1966) for rectangular and hollow cylindrical isotropic sections, and results obtained by Kennedy et al. (2011) for isotropic and layered isotropic sections. In the second part we compare the beam theory to full three-dimensional finite-element results. In the last part we present a parameter study to explore the behavior of

the homogenized stiffness and the strain moment correction matrix $\boldsymbol{C}_s$ for an angle-ply laminate.

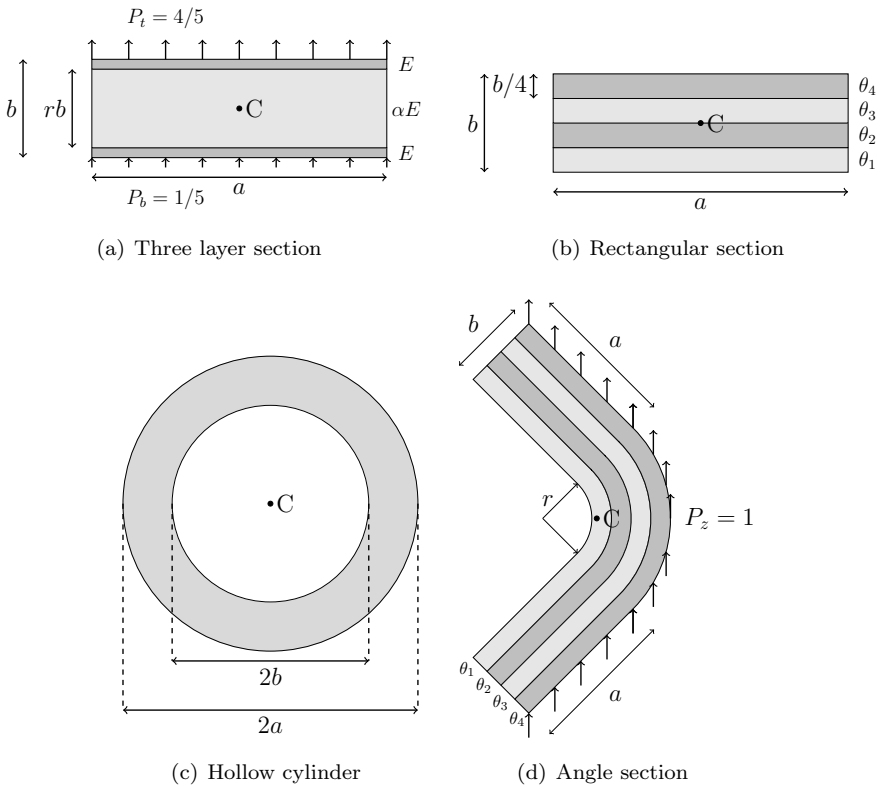

(a) Three layer section

(b) Rectangular section

(c) Hollow cylinder

(d) Angle section

Figure 3: The section geometries used for comparison. The centroid of each section is marked with a C.

The various cross-sections used here are shown in Figure 3. Note that some of the same variable names are used to refer to different dimensions for each cross-section. The particular variable definition should be clear from the context. The rectangular sections in Figures 3(a) and 3(b) have the same dimensions but have different material distributions. The three layer isotropic section in Figure 3(a) is designed to model a sandwich structure. The section has a core fraction r, and the ratio of the Young's modulus of the core to the face sheets is α. The four-layer beam shown in Figure 3(b) is composed of four orthotropic layers oriented at an angles θ_1 through θ_4 with respect to the x axis. The isotropic hollow circular section shown in Figure 3(c) has outer radius a and inner radius b. The angle section shown in Figure 3(d) is composed of four orthotropic layers oriented at angles θ_1 through θ_4.

5.1. Comparison with results from the literature

In this section we compare results from the beam theory-based finite-element approach presented above with results from the literature for an isotropic rectangular

section, the hollow isotropic circular section (Figure 3(c)) and the three layer section (Figure 3(a)).

5.1.1. Rectangular section

ν	k_{xz}	k_{xzFE}
0.1	0.839694656	0.839694656
0.2	0.845070423	0.845070423
0.3	0.849673203	0.849673203
0.4	0.853658537	0.853658537
b/a	k_t	k_{tFE}
1	0.843477276	0.843462636
1.5	0.722815002	0.722809435
2	0.548839062	0.548836918

Table 1: Comparison of Cowper's shear correction factor k_{xz} (44) and the torsion correction factor $k_t = J/(I_y + I_z)$, with finite-element calculations using a 31×31 node mesh with 10×10 bi-cubic elements for the rectangular section.

For a rectangular section composed of a single orthotropic material, Dharmarajan and McCutchen (1973) obtain a shear correction factors of

$$\begin{aligned} k_{xz} &= \frac{5E_x}{6E_x - \nu_{xz}G_{xz}}, \\ k_{xy} &= \frac{5E_x}{6E_x - \nu_{xy}G_{xy}}, \end{aligned} \tag{43}$$

where E_x, G_{xz} and G_{xy} are the material moduli in the beam axis and ν_{xz} and ν_{xy} are the Poisson ratios. For an isotropic material these formula simplify to Cowper's shear correction factor (Cowper, 1966):

$$k_{xz} = k_{xy} = \frac{10(1+\nu)}{12+11\nu}. \tag{44}$$

This factor does not depend on the dimensions of the rectangular section. Table 1 shows a comparison of the shear correction factor obtained from Cowper's formula (44) and finite-element based calculations for a range of Poisson's ratio $\nu = 0.1$, 0.2, 0.3 and 0.4. The finite-element calculations were performed on a 31×31 node mesh with 10×10 bi-cubic elements. Very good agreement was obtained.

The torsion strain correction factor k_t for an isotropic section is $k_t = J/(I_y + I_z)$, where J is the torsional stiffness of the section. Table 1 shows a comparison between the analytic formula obtained from Timoshenko and Goodier (1969) and the torsional strain moment correction, computed using the present approach with the previously described mesh for a range of depth-to-width ratios b/a.

b/a	k_{xz}	k_{xzFE}
0.75	0.547851299	0.547851299
0.25	0.771774856	0.771776170
0.15	0.837998917	0.838010143

Table 2: Comparison of Cowper's shear correction factor for a hollow cylinder with the present approach for a series of radius ratios. Finite-element calculations were performed on a 120×16 node mesh with 40×5 bi-cubic elements.

r	k_{xz}	k_{xzFE}	M^P	M^P_{FE}
0.25	0.714966088	0.714966088	1.385478992	1.38554164
0.5	0.744974670	0.744974670	3.041345731	3.04139193
0.75	0.825732040	0.825732040	2.767575511	2.76760868

Table 3: Comparison of the shear correction factor and stress moment correction for the isotropic three layer beam for a case with $\alpha = 0.1$

5.1.2. Hollow circular section

For a hollow, circular section, Cowper (1966) obtained a shear correction value of

$$k_{xz} = \frac{6(1+\nu)(1+m^2)^2}{(7+6\nu)(1+m^2)^2 + (20+12\nu)m^2}, \tag{45}$$

where $m = b/a$ is the ratio of the inner to the outer radius. The geometry of the hollow section is shown in Figure 3(c). Table 2 shows a comparison between Cowper's formula (45) and finite-element calculations performed on a 120×16 node mesh with 40×5 bi-cubic elements.

5.1.3. Three layer beam

Next, we consider a symmetric beam composed of three isotropic layers where the ratio of the Young's modulus of the core to the Young's modulus of the outer layers is α. The Poisson's ratio ν is the same in all layers. Using a plane stress assumption, the authors in previously published work (Kennedy et al., 2011), obtained an expression for the shear correction factor for beams of this construction as a function of core fraction r, and the ratio α. The shear correction factor in this case is,

$$k_{xz} = \frac{(1+\nu)(30r(s-1)+20)}{30(1+\nu)s - (6+8\nu) + 15(1+\nu)(1-s)(2+r^3-3r)}, \tag{46}$$

where $s = (1-(1-\alpha)r^2)/\alpha$. The authors (Kennedy et al., 2011), also derived expressions for the load-dependent axial and moment corrections that are too lengthy to report here.

Finite-element calculations were performed with a rectangular section with $a = 1$ and $b = 5$ using a 13×61 node mesh with 4×20 bi-cubic elements. Table 3 shows a numerical comparison for the case $\alpha = 0.1$. Exact agreement was obtained for the shear correction factor, and agreement to at least 4 digits was obtained for the stress moment

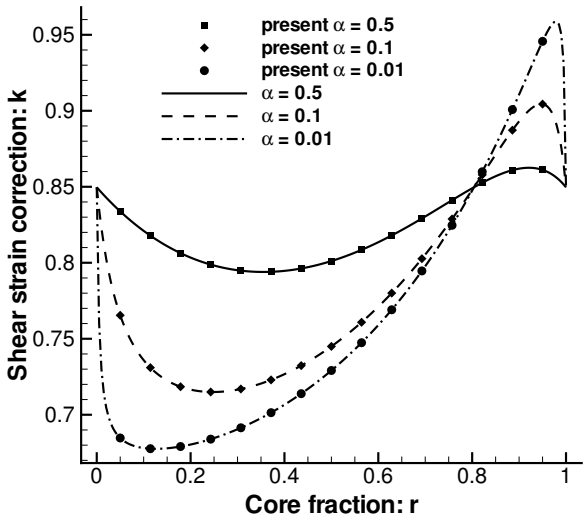

Figure 4: Comparison of the shear correction factor for the isotropic three layer beam. Finite-element results from the present approach are compared with Equation (46).

correction. Figure 4 shows a visual comparison between the shear correction factor (46) for the three layer beam, and the finite-element approach for $\alpha = 0.5$, 0.1, 0.01, and for a range of core ratios r between 0 and 1. Figure 5 shows a visual comparison of the load-dependent moment-correction obtained by the authors (Kennedy et al., 2011) and the present finite-element approach.

These results are especially interesting because the current approach uses a full three-dimensional through-thickness solution, while the authors (Kennedy et al., 2011) made a plane stress assumption. The full three-dimensional stress and strain distributions corresponding to shear and pressure loading are not constant in the direction transverse to the x-z plane. However, the additional contributions from the full three-dimensional solution cancel, and the plane stress formula (46) and present approach match.

5.2. Comparison with three-dimensional results

In this section we compare the beam theory results with calculations using a full three-dimensional finite-element model for the angle section shown in Figure 3(d), both for statically determinate and statically indeterminate boundary conditions. The beam under consideration is loaded with distributed surface tractions and end loads that include axial force, torque, bending moments and shear loads.

There are three main objectives in performing this study:

1. To compare the accuracy of the stress and strain reconstruction based on beam theory assumptions to the stress and strain distribution obtained using full three-dimensional finite-element calculations.
2. To quantify the errors introduced by neglecting both the strain correction error, $\tilde{\boldsymbol{e}}_r$, and the moments of the residual strain, $\mathcal{L}_s\tilde{\boldsymbol{\epsilon}}$.

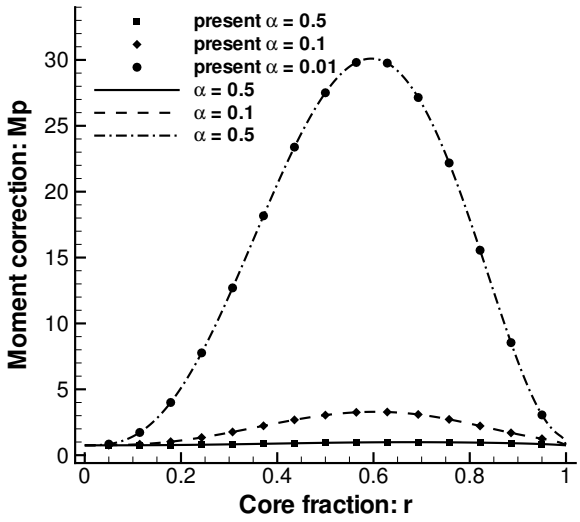

Figure 5: Comparison of the load-dependent moment correction for the isotropic three layer beam. Finite-element results from the present approach are compared with results from Kennedy et al. (2011).

Property	Value	Property	Value
E_1	164 GPa	G_{12}, G_{13}	21 GPa
E_2, E_3	8.3 GPa	G_{23}	12 GPa
ν_{12}, ν_{13}	0.34	ν_{23}	0.21

Table 4: The representative orthotropic stiffness properties used in the finite-element calculations. The relative stiffnesses are chosen to be representative of a graphite/epoxy composite system.

3. To assess the accuracy of the homogenized stiffness $\boldsymbol{D}$, the strain correction matrix $\boldsymbol{C}_s$ and the load-dependent corrections.

For this study, we use the angle-section geometry shown in Figure 3(d) with sectional dimensions $a = 3/2$, $b = 3/4$, $r = 1/2$, and overall beam length $L = 50$. The ply angles used for this case are $\theta = [45^o, -35^o, 35^o, -45^o]$, which is a balanced, anti-symmetric laminate. The tip of the beam at $x = L$, is loaded with axial, bending, torque and shear loads, $\boldsymbol{s} = [10, -625, 1250, 50, -25, 12.5] \times 10^6$, and a constant traction is applied to the beam such that $P_z = 1$, $P_y = 0$. The traction is distributed on the outer surface of the section and is only applied in the z direction with $t_z = 2/(\pi(r + b) + 4a)$ and $t_y = 0$. There is also a non-zero P_x force due to the distribution of the traction on the section. The material properties for the beam are listed in Table 4. The relative magnitudes of the stiffnesses properties are chosen to be representative of a high modulus graphite/epoxy system. Note that the dimensions of the beam are selected to facilitate three-dimensional modeling using finite-elements and are not representative of a physical beam. Using smaller, more realistic ply thicknesses would increase the computational cost of the analysis, as more elements would be required to keep the element aspect ratio

within a reasonable range. This test case should be viewed as a convenient model for comparison purposes.

To test different aspects of the present beam theory, we impose two different sets of boundary conditions on the same finite-element model. These two sets of boundary conditions result in two separate finite-element problems, which we denote B1 and B2. The boundary conditions for case B1 are statically determinate. All displacements at the beam root, $x = 0$, are completely fixed, while the displacements at the tip, $x = L$, remain free. The boundary conditions for case B2 are statically indeterminate. In this case, the beam root is completely fixed, while at the tip only the axial displacement $u = 0$ is fixed. For case B2, the axial force and bending moments at the tip are not applied.

To model the beam using three-dimensional finite-elements, we use a mesh with $289 \times 97 \times 25$ nodes, where the three dimensions are the x-direction, the direction along the contour of the section, and through the thickness, respectively. This results in a problem with 2 102 475 degrees of freedom. We use $96 \times 32 \times 8$ tri-cubic elements resulting in two elements through the thickness of each ply. This large high-order finite-element model is employed to accurately model the through-section stresses and limit the effect of discretization error. Such a large high-order finite-element problem must be solved by a specialized finite-element code. To solve these beam problems, we use the Toolkit for the Analysis of Composite Structures (TACS) (Kennedy and Martins, 2010), a parallel finite-element code specially designed for the analysis of composite structures. We solve these beam problems using 48 processors. The total solution time is approximately 10 minutes of wall time corresponding to 8 hours of CPU time.

To model the beam described above using the present beam theory, we employ a fundamental state analysis with a sectional nodal mesh of 97×25 nodes along the contour of the section and through the thickness, with a 32×8 bi-cubic element mesh. This problem contains 7 287 degrees of freedom for the section, including nodal degrees of freedom, invariants, and the Lagrange multipliers. For the beam analysis, we use 96, displacement-based, Timoshenko-type cubic elements along the length of the beam. These elements have been modified to use load-dependent strain and stress moment corrections and to accept the non-symmetric stiffness relationship. All beam theory computations, including the determination of the fundamental states and solution of the beam problem, take less than 15 seconds on a desktop computer with a single processor. This is a vast difference in computation effort: the full three-dimensional problem requires approximately 1920 times more computational effort compared to the beam theory calculations.

For the angle section described above, the homogenized stiffness matrix $\boldsymbol{D}$, normalized by the Young's modulus E_1 is,

$$\frac{\boldsymbol{D}}{E_1} = \begin{bmatrix} 0.415965 & 0 & 0.0213894 & 0.0811495 & -0.0517882 & 0 \\ 0 & 0.407744 & 0 & 0 & 0 & -0.0254769 \\ 0.00488284 & 0 & 0.396857 & 0.00914746 & 0.00971687 & 0 \\ 0.0107402 & 0 & 0.0402207 & 0.157807 & 0.0516136 & 0 \\ 0.00482657 & 0 & 0.0519170 & 0.0318435 & 0.193637 & 0 \\ 0 & -0.00577706 & 0 & 0 & 0 & 0.191402 \end{bmatrix}.$$

Note that the y components of bending κ_y and shear e_{xz} are decoupled. This decoupling is due both to the geometry of the section and the layup of the beam. The strain

correction matrix $\boldsymbol{C}_s$ is,

$$\boldsymbol{C}_s = \begin{bmatrix} 1 & 0 & 0 & 0 & 0 & 0 \\ 0 & 1 & 0 & 0 & 0 & 0 \\ 0 & 0 & 1 & 0 & 0 & 0 \\ 0.0670449 & 0 & -0.0202593 & 0.399008 & 0.396402 & 0 \\ -0.0351000 & 0 & -0.0891052 & 0.311563 & 0.595588 & 0 \\ 0 & 0.00225714 & 0 & 0 & 0 & 0.542370 \end{bmatrix}.$$

Note again that there is coupling between the y component of shear and bending and the z component of shear and torsion.

The strain moment correction $\boldsymbol{e}_{FL}^{(1)}$ and stress-moment correction $\boldsymbol{s}_{FL}^{(1)}$ are,

$$\boldsymbol{e}_{FL}^{(1)} = \begin{bmatrix} 0 & 0 & 0 & 0 & 0 & 4.47333376 \times 10^{-6} \end{bmatrix}^T,$$
$$\frac{\boldsymbol{s}_{FL}^{(1)}}{E_1} = \begin{bmatrix} 0 & 7.12433 \times 10^{-4} & 0 & 0 & 0 & -3.87965 \times 10^{-4} \end{bmatrix}^T.$$

While the stress and strain moment corrections are small in magnitude, ignoring these terms produces measurable errors when the beam theory calculations are compared with finite-element results.

5.2.1. Statically determinate beam

In this section we examine the results from the problem B1. Since this case is statically determinate, the stress moments can be determined from the equilibrium equations (9) alone. Therefore, the results in this section must be interpreted from the point of view of known stress resultants, but unknown strain moments.

First, we examine the accuracy of the stress and strain reconstruction from Equation (11). Instead of plotting the error in each of the 12 components of stress and strain, we use the following quantity to concisely present a single error measure per unit length of the beam:

$$\Delta \mathrm{SE}_{\mathrm{rel}}(x) = \frac{\int_\Omega \tilde{\boldsymbol{\epsilon}}_{\mathrm{3D}} \cdot \tilde{\boldsymbol{\sigma}}_{\mathrm{3D}} \, d\Omega}{\int_\Omega \boldsymbol{\epsilon}_{\mathrm{3D}} \cdot \boldsymbol{\sigma}_{\mathrm{3D}} \, d\Omega}. \tag{47}$$

In the above equation, $\boldsymbol{\sigma}_{\mathrm{3D}}$ and $\boldsymbol{\epsilon}_{\mathrm{3D}}$ are the stress and strain solutions from the three-dimensional finite-element problem, while $\tilde{\boldsymbol{\sigma}}_{\mathrm{3D}}$ and $\tilde{\boldsymbol{\epsilon}}_{\mathrm{3D}}$ are the differences between the three-dimensional solution and the beam theory reconstruction, and therefore represent approximations of the true stress and strain residuals, $\tilde{\boldsymbol{\sigma}}$ and $\tilde{\boldsymbol{\epsilon}}$, in Equation (11). The quantity $\Delta \mathrm{SE}_{\mathrm{rel}}$ is the strain energy of the difference between the beam theory and the full three-dimensional solution, per unit length of the beam, normalized by the sectional strain energy at the current x position. An error in one component of the stress and strain produces a measurable error in $\Delta \mathrm{SE}_{\mathrm{rel}}$. As a result, $\Delta \mathrm{SE}_{\mathrm{rel}}$ shows the accuracy of all components of the stress and strain reconstruction.

Figure 6 shows $\Delta \mathrm{SE}_{\mathrm{rel}}$ as a function of x-location for the case B1. $\Delta \mathrm{SE}_{\mathrm{rel}}$ is largest at the ends of the beam and decreases rapidly towards the center of the beam. This result demonstrates the high degree of accuracy of the stress and strain reconstruction just a few thicknesses away from the ends of the beam.

Next, we compare the strain moments computed from the full three-dimensional

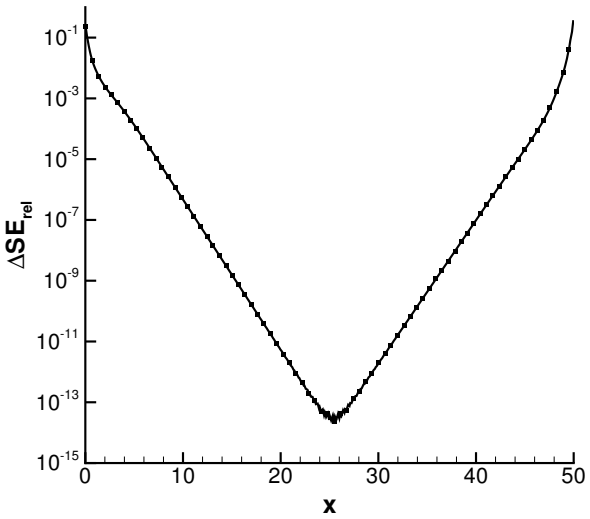

Figure 6: The integrated strain energy of the difference between the beam theory reconstruction and the three-dimensional, finite-element solution. The results show excellent agreement away from the ends of the beam.

theory to those computed using the beam theory. This study tests how accurately the strain moments can be determined from the known stress moments. The accuracy of the strain moments, in turn, depends on the accuracy of the flexibility matrix $\boldsymbol{E}$ (15) and the load-dependent strain corrections (29). Figure 7(a) shows a comparison of the e_x, κ_z and κ_y components of the strain moments between the beam theory and three-dimensional finite-element results. The relative error between beam theory and three-dimensional finite-element results for the e_x, κ_z and κ_y components are shown in Figure 7(b), where each variable is normalized by the maximum absolute value of the corresponding strain moment over the length of the beam. Figure 8(a) shows a comparison between the e_t, e_{xz} and e_{xy} components of the strain moments for the beam theory and three-dimensional finite-element results. Figure 8(b) shows the relative error between the beam theory and the three-dimensional finite-element results, normalized by the maximum absolute value of the strain moment component over the length of the beam. The strain moment comparisons in Figures 7 and 8 demonstrate agreement to a relative tolerance of 10^{-6} between the full three-dimensional finite-element results and the present beam theory, over the middle portion of the beam. The differences near the ends of the beam cannot be predicted without recourse to full three-dimensional calculations.

Moments of the strain residuals. One of the key assumptions in the beam theory presented above is that the moments of the residual strains, $\mathcal{L}_s\tilde{\boldsymbol{\epsilon}}$ are small. Here we test this assumption using the full three-dimensional finite-element solution to problem B1. To evaluate $\mathcal{L}_s\tilde{\boldsymbol{\epsilon}}$ we first use the beam theory to determine the flexibility matrix $\boldsymbol{E}$ and

the strain moment contributions from the externally applied loads:

$$\boldsymbol{e}_P = P_z \boldsymbol{L}_s \boldsymbol{\epsilon}_{FL}^{(1)}(y,z),$$

where $P_z = 1$ is the magnitude of the applied load and $\boldsymbol{L}_s$ is the discrete analogue of $\mathcal{L}_s$. Based on Equation (16), the discrete analogue of $\mathcal{L}_s\tilde{\boldsymbol{\epsilon}}$ can be determined using

$$\boldsymbol{L}_s\tilde{\boldsymbol{\epsilon}}|_{3\mathrm{D}} = \boldsymbol{L}_s\boldsymbol{\epsilon}_{3\mathrm{D}} - \boldsymbol{E}\boldsymbol{L}_s\boldsymbol{\sigma}_{3\mathrm{D}} - \boldsymbol{e}_P, \tag{48}$$

where the $\boldsymbol{\epsilon}_{3\mathrm{D}}$ and $\boldsymbol{\sigma}_{3\mathrm{D}}$ are the three-dimensional finite-element stress and strain fields respectively.

Figure 9 shows the e_x, k_z and e_{xz} components of $\boldsymbol{L}_s\tilde{\boldsymbol{\epsilon}}|_{3\mathrm{D}}$ normalized by the maximum absolute value of the strain moment component over the domain. The remaining components of the moments of the residual strain exhibit similar behavior. At the edges of the beam the contribution of the moments of the strain residuals are significant, however their influence decreases rapidly away from the ends of the beam. Note that in Figure 9 the oscillations at the center of the beam in the e_x and e_{xz} components are due to the finite precision of the finite-element solutions. In these regions, the moments of the strain residuals are essentially zero.

Strain correction error. The strain correction error $\tilde{\boldsymbol{e}}_r$ from Equation (25) represents the difference between the actual strain moments and the corrected strain moments. Here, we examine an approximation of the strain correction error obtained from the full three-dimensional finite-element solution of problem B1. This case verifies the accuracy of the correction flexibility matrix $\tilde{\boldsymbol{E}}$ and the load-dependent strain correction contribution $\tilde{\mathcal{L}}\tilde{u}_{FL}^{(k)}$ terms. Note that no correction is required for the strain moments e_x, κ_z and κ_y, so here we examine the behavior of the components e_t, e_{xz} and e_{xy}.

In order to obtain an approximation of $\tilde{\boldsymbol{e}}_r$, we first compute the flexibility correction matrix $\tilde{\boldsymbol{E}}$ (20) and the load-dependent strain correction $\tilde{\boldsymbol{L}}U_{FL}^{(1)}$ using the present beam theory. Rearranging Equation (25), we obtain,

$$\tilde{\boldsymbol{e}}_r|_{3\mathrm{D}} = \boldsymbol{L}_s\boldsymbol{\epsilon}_{3\mathrm{D}} - \boldsymbol{A}\boldsymbol{L}_\epsilon\boldsymbol{u}_{03\mathrm{D}} - \tilde{\boldsymbol{E}}\boldsymbol{L}_s\boldsymbol{\sigma}_{3\mathrm{D}} - P_z\tilde{\boldsymbol{L}}U_{FL}^{(1)}(y,z), \tag{49}$$

where $\tilde{\boldsymbol{e}}_r|_{3\mathrm{D}}$ is the finite-element approximation of $\tilde{\boldsymbol{e}}_r$. Here, $\boldsymbol{u}_{03\mathrm{D}}$ is the finite-element approximation of the normalized strain moments $\boldsymbol{u}_0(x)$ and $\boldsymbol{\epsilon}_{3\mathrm{D}}$ is the finite-element strain distribution.

Instead of plotting $\tilde{\boldsymbol{e}}_r|_{3\mathrm{D}}$ directly, we plot the relative values in Figure 10, normalized by the maximum absolute value of the strain moment along the length of the beam. The results shown in Figure 10 are similar in many respects to the moments of the strain residuals shown in Figure 9. The strain correction error is greatest near the ends of the beam and quickly decays towards the middle of the beam. The largest relative error is in the e_{xy} component of the relative strain correction error, however all components fall below 10^{-5} over the center portion of the beam. This suggests that it is reasonable to neglect $\tilde{\boldsymbol{e}}_r$ at a sufficient distance from the ends of the beam.

5.2.2. Statically indeterminate beam

In this section, we examine the results from the statically indeterminate case B2. This case demonstrates the overall capabilities of the beam theory and quantifies the

errors introduced by neglecting both the strain correction error $\tilde{\boldsymbol{e}}_r$, and the moments of the strain residual $\mathcal{L}_s\tilde{\boldsymbol{\epsilon}}$.

Figure 11 shows the strain-energy based error measure (47) for the statically indeterminate beam problem. The error measure decreases rapidly away from the ends of the beam, but only falls to between 10^{-4} and 10^{-5} over the center portion of the beam. Clearly, the beam theory reconstruction and the finite-element results do not match as closely as the statically determinate case B1. This small error in $\Delta\text{SE}_{\text{rel}}$ is due to an error in the prediction of the stress and strain moments due to neglecting the contributions $\tilde{\boldsymbol{e}}_r$ and $\mathcal{L}_s\tilde{\boldsymbol{\epsilon}}$.

Figure 12(a) shows a comparison between the beam theory results and the three-dimensional finite-element results for the strain moment components e_x, κ_z and κ_y. The results match closely to plotting precision. However, Figure 12(b) shows the relative error between the beam theory and the finite-element results normalized by the maximum absolute value of each component of the strain moment over the length of the beam. This relative error decreases away from the ends of the beam but reaches a constant value over the middle portion of the beam. Figure 13 shows similar behavior for the e_t, e_{xz} and e_{xy} components of the strain moments. Based on the previous results for the statically determinate beam that were used to verify the present approach, we can conclude that these errors must be a product of the assumptions that both the moments of the strain residuals and the strain correction error can be neglected. The result of the violation of these assumptions near the end of the beam produces a small but measurable error between the beam theory and the three-dimensional results. The largest relative error occurs for e_x and is roughly 2%.

Figure 14 shows a comparison of the volumetric strain for the three-dimensional and beam theory solutions at the middle of the beam, $x = 25$. While there are some small differences between the beam theory and full three-dimensional solution resulting in non-zero $\Delta\text{SE}_{\text{rel}}$, these differences are not significant from an engineering perspective.

5.3. Angle-ply study

Next, we examine the behavior of the homogenized stiffness matrix $\boldsymbol{D}$, and the strain correction matrix $\boldsymbol{C}_s$ for a four ply rectangular beam with $a = 4$, $b = 2$, and with an angle-ply layup: $[\theta, -\theta, \theta, -\theta]$. Here we use the material properties listed in Table (4). All calculations below are performed on a 31×25 mesh with 10×8 bi-cubic elements.

In this case, $\boldsymbol{D}$ has non-zero components along the diagonal and off-diagonal components at $\boldsymbol{D}_{41}$, $\boldsymbol{D}_{14}$, $\boldsymbol{D}_{62}$, $\boldsymbol{D}_{26}$ and $\boldsymbol{D}_{35}$. The strain correction matrix $\boldsymbol{C}_s$ has non-zero diagonal components with additional off-diagonal components $\boldsymbol{C}_{s41}$ and $\boldsymbol{C}_{s62}$. Figure 15 shows the variation of the $\boldsymbol{D}_{44}$, $\boldsymbol{D}_{55}$ and $\boldsymbol{D}_{66}$ with respect to ply angles in the range $\theta = 0^o$ to 90^o, normalized by the shear modulus G_{12}. $\boldsymbol{D}_{44}$, $\boldsymbol{D}_{55}$ and $\boldsymbol{D}_{66}$ represent the torsional, shear, and transverse shear components of the homogenized stiffness matrix respectively. The homogenized values all start from the value G_{12} at $\theta = 0$. The component $\boldsymbol{D}_{66}$ increases from G_{12} to a maximum at 45^o and returning to a value of G_{12} at $\theta = 90^o$. The transverse shear component $\boldsymbol{D}_{55}$ reaches the value G_{23} at $\theta = 90^o$. The torsional component $\boldsymbol{D}_{44}$ takes an intermediate value between G_{12} and G_{23} at $\theta = 90^o$. Figure 16 shows the off-diagonal components of the homogenized stiffness $\boldsymbol{D}_{41}$, $\boldsymbol{D}_{14}$, $\boldsymbol{D}_{62}$, $\boldsymbol{D}_{26}$ and $\boldsymbol{D}_{35}$. It is important to note that the off-diagonal stiffnesses are of similar magnitude to the diagonal stiffness.

Figure 17 shows the variation of the diagonal components of $\boldsymbol{C}_s$ corresponding to shear, transverse shear, and torsion. The strain moment corrections for the shear and transverse shear take on values between about 0.83 and 0.89. The shear strain correction for torsion takes on much lower values between about 0.55 and 0.68. At $\theta = 0^o$ and $\theta = 90^o$, the beam is orthotropic, the matrix $\boldsymbol{C}_s$ is diagonal, and the shear correction factors match the formula (43) derived by Dharmarajan and McCutchen (1973). Figure 18 shows the off-diagonal components of the strain correction matrix $\boldsymbol{C}_s$ as a function of θ. The non-zero components $\boldsymbol{C}_{s41}$ and $\boldsymbol{C}_{s62}$ represent a coupling between axial strain and torsional strain, and bending about the y-axis and transverse shear. These values are between 0 to 18% of the strain corrections applied to the diagonal components.

6. Conclusions

In this paper we presented a homogenization-based theory for three-dimensional beams. The theory uses a kinematic description of the beam based on normalized displacement moments. The stress and strain distribution in the beam is approximated based on a linear combination of a hierarchy of axially-invariant stress and strain solutions called the fundamental states. The fundamental state solutions are used to construct a constitutive relationship between moments of stress and moments strain. The fundamental states are also used to determine a strain correction matrix that modifies the strain moments predicted by the normalized displacement moments. For isotropic beams with symmetric cross-sections, the present beam theory takes the form of classical Timoshenko beam theory with additional load-dependent stress and strain corrections. For arbitrary, anisotropic sections, the homogenized stiffness matrix becomes fully populated and all components of the stress resultants are coupled.

In addition, we presented a finite-element based method for the calculation of the fundamental state solutions, and verified this approach with three-dimensional finite-element calculations. We demonstrated excellent agreement between the stress and strain distributions for statically determinate and statically indeterminate problems, achieving extremely high accuracy away from the ends of the beam. For statically determinate problems, the relative error of all strain moment components at the center of the beam was less than 10^{-6}, while for the statically indeterminate beam, the maximum relative error was 10^{-2}. The larger error for the statically indeterminate case was attributed to the moments of the strain residuals and the strain correction error. Despite this error, the stress and strain reconstruction remains sufficiently accurate for engineering purposes. In addition, the finite-element based beam theory calculations required three orders of magnitude less computational time compared to three-dimensional finite-element computations. These characteristics make the beam theory an attractive approach for accurate through-thickness stress and strain prediction in composite beams.

Acknowledgments

Some of the computations herein were performed on the General Purpose Cluster supercomputer at the SciNet HPC Consortium. SciNet is funded by the Canada Foundation for Innovation under the auspices of Compute Canada, the Government of Ontario, Ontario Research Fund - Research Excellence, and the University of Toronto.

References

Bank, L. C., 1987. Shear coefficients for thin-walled composite beams. Composite Structures 8 (1), 47 – 61.
URL http://www.sciencedirect.com/science/article/B6TWP-4816PHD-1G/2/438b1fa03e76ce7248b14ed771e3b28b

Bank, L. C., Melehan, T. P., 1989. Shear coefficients for multicelled thin-walled composite beams. Composite Structures 11 (4), 259 – 276.
URL http://www.sciencedirect.com/science/article/B6TWP-47S102T-8/2/e667a575b8e6a975bad07f67ae79d933

Berdichevskii, V. L., 1979. Variational-asymptotic method of constructing a theory of shells. Journal of Applied Mathematics and Mechanics 43 (4), 711 – 736.
URL http://www.sciencedirect.com/science/article/pii/0021892879901576

Carrera, E., 2003. Historical review of zig-zag theories for multilayered plates and shells. Applied Mechanics Reviews 56 (3), 287–308.
URL http://link.aip.org/link/?AMR/56/287/1

Carrera, E., Giunta, G., 2010. Refined beam theories based on a unified formulation. International Journal of Applied Mechanics 2, 117–143.

Carrera, E., Giunta, G., Nali, P., Petrolo, M., 2010a. Refined beam elements with arbitrary cross-section geometries. Computers & Structures 88 (5-6), 283 – 293.
URL http://www.sciencedirect.com/science/article/pii/S0045794909002752

Carrera, E., Giunta, G., Petrolo, M., 2010b. Beam Structures: Classical and Advanced Theories. John Wiley & Sons.

Carrera, E., Petrolo, M., 2011. On the effectiveness of higher-order terms in refined beam theories. Journal of Applied Mechanics 78 (2), 021013.
URL http://link.aip.org/link/?AMJ/78/021013/1

Carrera, E., Petrolo, M., Nali, P., 2011. Unified formulation applied to free vibrations finite element analysis of beams with arbitrary section. Shock and Vibration 18 (3), 285–502.

Cesnik, C. E. S., Hodges, D. H., 1997. VABS: A new concept for composite rotor blade cross-sectional modeling. Journal of the American Helicopter Society 42 (1), 27–38.
URL http://dx.doi.org/doi/10.4050/JAHS.42.27

Cowper, G., 1966. The shear coefficient in Timoshenko's beam theory. Journal of Applied Mechanics 33 (5), 335–340.

Dharmarajan, S., McCutchen, H., 1973. Shear coefficients for orthotropic beams. Journal of Composite Materials 7 (4), 530–535.
URL http://jcm.sagepub.com/content/7/4/530.short

Dong, S., Alpdogan, C., Taciroglu, E., 2010. Much ado about shear correction factors in Timoshenko beam theory. International Journal of Solids and Structures 47 (13), 1651 – 1665.
URL http://www.sciencedirect.com/science/article/B6VJS-4YH56DC-2/2/21f0dd8f7d8e2e484f97b062d810c136

Dong, S. B., Kosmatka, J. B., Lin, H. C., 2001. On Saint–Venant's problem for an inhomogeneous, anisotropic cylinder—Part I: Methodology for Saint–Venant solutions. Journal of Applied Mechanics 68 (3), 376–381.
URL http://link.aip.org/link/?AMJ/68/376/1

El Fatmi, R., 2007a. Non-uniform warping including the effects of torsion and shear forces. Part I: A general beam theory. International Journal of Solids and Structures 44 (18-19), 5912 – 5929.
URL http://www.sciencedirect.com/science/article/pii/S0020768307000728

El Fatmi, R., 2007b. Non-uniform warping including the effects of torsion and shear forces. Part II: Analytical and numerical applications. International Journal of Solids and Structures 44 (18-19), 5930 – 5952.
URL http://www.sciencedirect.com/science/article/pii/S002076830700073X

El Fatmi, R., Zenzri, H., 2002. On the structural behavior and the Saint–Venant solution in the exact beam theory: Application to laminated composite beams. Computers & Structures 80 (16-17), 1441 – 1456.
URL http://www.sciencedirect.com/science/article/pii/S0045794902000901

El Fatmi, R., Zenzri, H., 2004. A numerical method for the exact elastic beam theory. Applications to homogeneous and composite beams. International Journal of Solids and Structures 41 (9-10), 2521 – 2537.
URL http://www.sciencedirect.com/science/article/pii/S0020768303007108

Gruttmann, F., Wagner, W., 2001. Shear correction factors in Timoshenko's beam theory for arbitrary shaped cross-sections. Computational Mechanics 27, 199–207, 10.1007/s004660100239.
URL http://dx.doi.org/10.1007/s004660100239

Guiamatsia, I., 2010. A new approach to plate theory based on through-thickness homogenization. International Journal for Numerical Methods in Engineering.
URL http://dx.doi.org/10.1002/nme.2934

Guiamatsia, I., Hansen, J. S., 2004. A homogenization-based laminated plate theory. ASME Conference Proceedings 2004 (47004), 421–436.
URL http://link.aip.org/link/abstract/ASMECP/v2004/i47004/p421/s1

Hansen, J., Kennedy, G. J., de Almeida, S. F. M., 2005. A homogenization-based theory for laminated and sandwich beams. In: 7th International Conference on Sandwich Structures. Aalborg University, Aalborg, Denmark, pp. 221–230.

Hansen, J. S., Almeida, S. d., April 2001. A theory for laminated composite beams. Tech. rep., Instituto Tecnológico de Aeronáutica.

Hutchinson, J. R., 2001. Shear coefficients for Timoshenko beam theory. Journal of Applied Mechanics 68 (1), 87–92.
URL http://link.aip.org/link/?AMJ/68/87/1

Ieşan, D., 1986a. On Saint–Venant's problem. Archive for Rational Mechanics and Analysis 91, 363–373, 10.1007/BF00282340.
URL http://dx.doi.org/10.1007/BF00282340

Ieşan, D., 1986b. On the theory of uniformly loaded cylinders. Journal of Elasticity 16, 375–382, 10.1007/BF00041762.
URL http://dx.doi.org/10.1007/BF00041762

Kennedy, G. J., Hansen, J. S., Martins, J. R. R. A., 2011. A Timoshenko beam theory with pressure corrections for layered orthotropic beams. International Journal of Solids and Structures 48 (16-17), 2373 – 2382.
URL http://www.sciencedirect.com/science/article/pii/S0020768311001466

Kennedy, G. J., Martins, J. R. R. A., September 2010. Parallel solution methods for aerostructural analysis and design optimization. In: Proceedings of the 13th AIAA/ISSMO Multidisciplinary Analysis Optimization Conference. Fort Worth, TX, AIAA 2010-9308.

Kosmatka, J. B., Lin, H. C., Dong, S. B., 2001. On Saint–Venant's problem for an inhomogeneous, anisotropic cylinder—Part II: Cross-sectional properties. Journal of Applied Mechanics 68 (3), 382–391.
URL http://link.aip.org/link/?AMJ/68/382/1

Ladevéze, P., Sanchez, P., Simmonds, J. G., 2002. On application of the exact theory of elastic beams. In: Durban, D., Givoli, D., Simmonds, J. G., Gladwell, G. M. L. (Eds.), Advances in the Mechanics of Plates and Shells. Vol. 88 of Solid Mechanics and Its Applications. Springer Netherlands, pp. 181–196, 10.1007/0-306-46954-5-12.
URL http://dx.doi.org/10.1007/0-306-46954-5-12

Ladevéze, P., Simmonds, J., 1998. New concepts for linear beam theory with arbitrary geometry and loading. European Journal of Mechanics - A/Solids 17 (3), 377 – 402.
URL http://www.sciencedirect.com/science/article/pii/S099775389880051X

Lekhnitskii, S., 1935. Strength calculation of composite beams. Vestnik inzhen i tekhnikov (9).

Librescu, L., Song, O., 2006. Thin-walled composite beams: theory and application. Solid mechanics and its applications. Springer.
URL http://books.google.ca/books?id=Ll4I8mD8Ix4C

Lo, K. H., Christensen, R. M., Wu, E. M., 1977a. A high-order theory of plate deformation—part 1: Homogeneous plates. Journal of Applied Mechanics 44 (4), 663–668.
URL http://link.aip.org/link/?AMJ/44/663/1

Lo, K. H., Christensen, R. M., Wu, E. M., 1977b. A high-order theory of plate deformation—part 2: Laminated plates. Journal of Applied Mechanics 44 (4), 669–676.
URL http://link.aip.org/link/?AMJ/44/669/1

Love, A. E. H., 1920. A Treatise on the Mathematical Theory of Elasticity, 3rd Edition. Cambridge University Press.

Mason, W., Herrmann, L., 1968. Elastic shear analysis of general prismatic beams. Journal Engineering Mechanics Division ASCE 94, 965–983.

Pagano, N. J., Pipes, R. B., 1971. The influence of stacking sequence on laminate strength. Journal of Composite Materials 5 (1), 50–57.

Pipes, R. B., Pagano, N., 1970. Interlaminar stresses in composite laminates under uniform axial exten-

sion. Journal of Composite Materials 4 (4), 538–548.
URL http://jcm.sagepub.com/content/4/4/538.abstract

Popescu, B., Hodges, D. H., 2000. On asymptotically correct Timoshenko-like anisotropic beam theory. International Journal of Solids and Structures 37 (3), 535 – 558.
URL http://www.sciencedirect.com/science/article/B6VJS-3XM2SF5-7/2/aefcc4a6cdb0debe8fe1d1f196b8e623

Prescott, J., 1942. Elastic waves and vibrations of thin rods. Philosophical Magazine 33, 703–754.
URL http://www.informaworld.com/10.1080/14786444208521261

Reddy, J. N., 1987. A generalization of two-dimensional theories of laminated composite plates. Communications in Applied Numerical Methods 3 (3), 173–180.
URL http://dx.doi.org/10.1002/cnm.1630030303

Schramm, U., Kitis, L., Kang, W., Pilkey, W. D., 1994. On the shear deformation coefficient in beam theory. Finite Elements in Analysis and Design 16 (2), 141 – 162.
URL http://www.sciencedirect.com/science/article/B6V36-47X88CD-4W/2/b29277277d1bae17f590c51c25db3ba4

Stephen, N. G., 1980. Timoshenko's shear coefficient from a beam subjected to gravity loading. Journal of Applied Mechanics 47 (1), 121–127.
URL http://link.aip.org/link/?AMJ/47/121/1

Stephen, N. G., 2001. Discussion: "Shear coefficients for Timoshenko beam theory". Journal of Applied Mechanics 68 (11), 959–960.

Stephen, N. G., Levinson, M., 1979. A second order beam theory. Journal of Sound and Vibration 67 (3), 293–305.

Timoshenko, S., Goodier, J., 1969. Theory of elasticity. McGraw-Hill classic textbook reissue series. McGraw-Hill.

Timoshenko, S. P., 1921. On the correction for shear of the differential equation for transverse vibrations of prismatic bars. Philosophical Magazine 41, 744–746.

Timoshenko, S. P., 1922. On the transverse vibrations of bars of uniform cross-section. Philosophical Magazine 43, 125 – 131.

Yu, W., Hodges, D. H., Volovoi, V., Cesnik, C. E. S., 2002a. On Timoshenko-like modeling of initially curved and twisted composite beams. International Journal of Solids and Structures 39 (19), 5101 – 5121.
URL http://www.sciencedirect.com/science/article/pii/S0020768302003992

Yu, W., Volovoi, V. V., Hodges, D. H., , Hong, X., 2002b. Validation of the variational asymptotic beam sectional analysis. AIAA Journal 40 (10), 2105–2112.

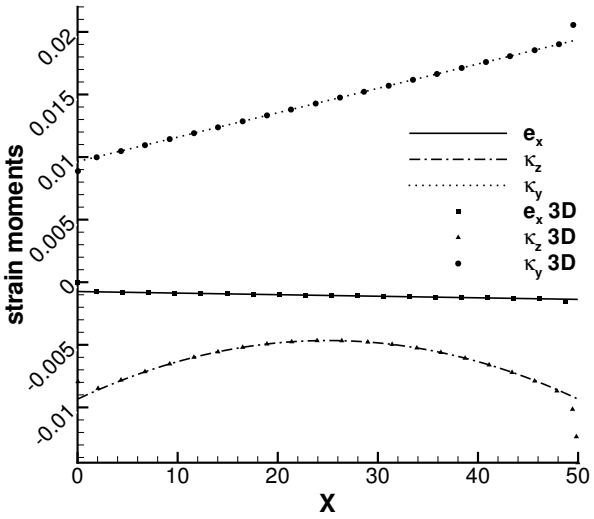

(a) Strain moments

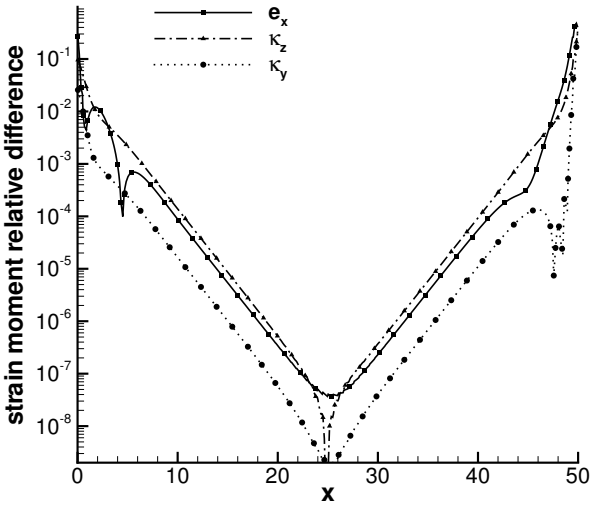

(b) Relative error

Figure 7: The first three components of the strain moments and the relative error between the beam theory prediction and the full three-dimensional calculations. The relative error is defined as $e_{\mathrm{rel}} = |e - e_{3\mathrm{D}}|/\max(|e_{3\mathrm{D}}|)$.

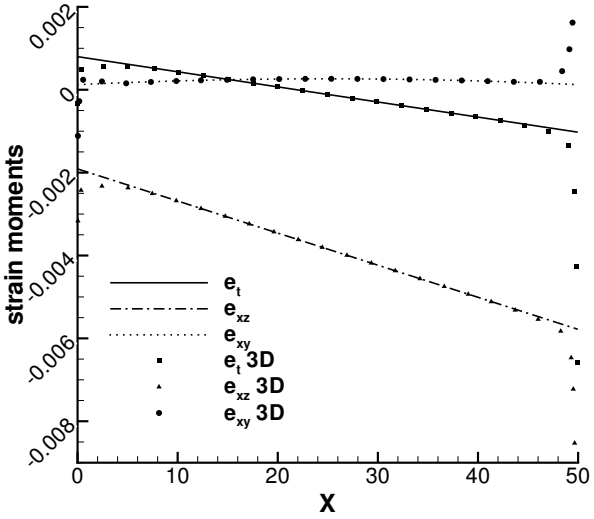

(a) Strain moments

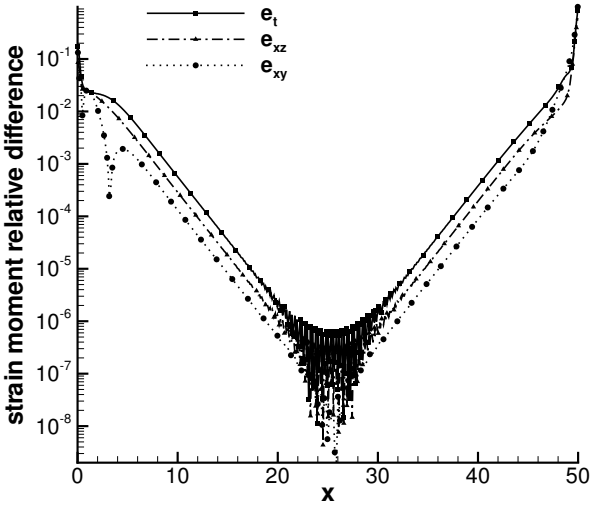

(b) Relative error

Figure 8: The last three components of the strain moments and the relative error between the beam theory prediction and the full three-dimensional calculations. The relative error is defined as $e_{\mathrm{rel}} = |e - e_{3\mathrm{D}}|/\max(|e_{3\mathrm{D}}|)$.

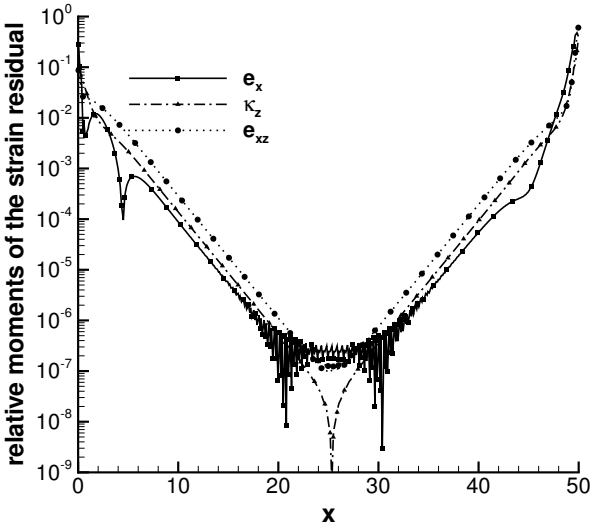

Figure 9: Components of the relative moments of the strain residual $\boldsymbol{L}_s\tilde{\boldsymbol{\epsilon}}|_{3\mathrm{D}}$ normalized by the maximum absolute values of the strain moment over the domain. These quantities are computed from a combination of the finite-element solution and the beam theory using Equation (48). These components are representative of the remaining components.

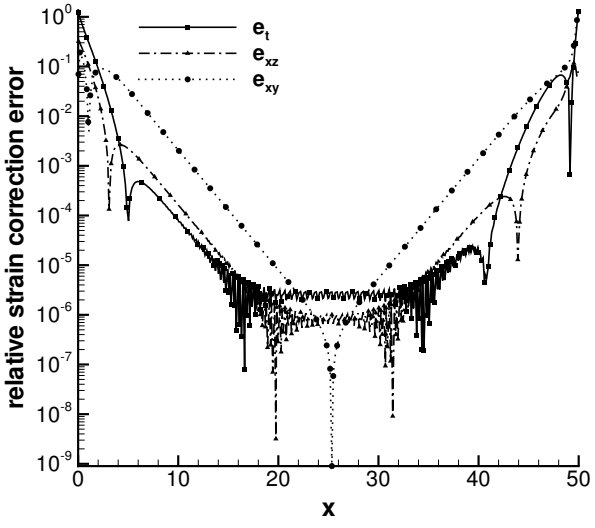

Figure 10: Components of the relative strain correction error. The strain correction error is normalized by the maximum absolute values of the strain moment over the domain.

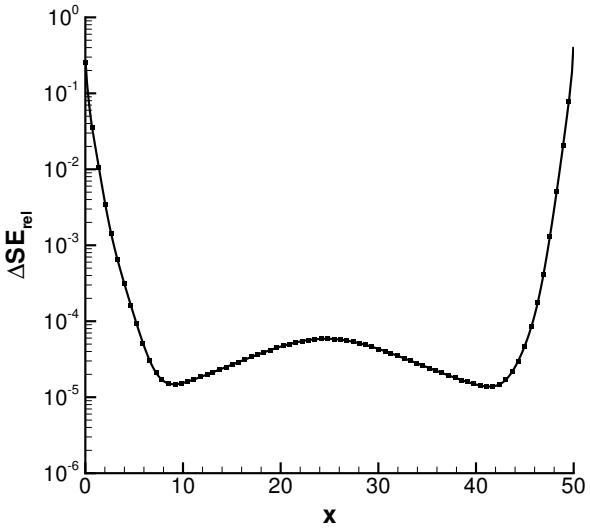

Figure 11: The integrated strain energy of the difference between the beam theory reconstruction and the three-dimensional, finite-element solution. The results show excellent agreement away from the ends of the beam.

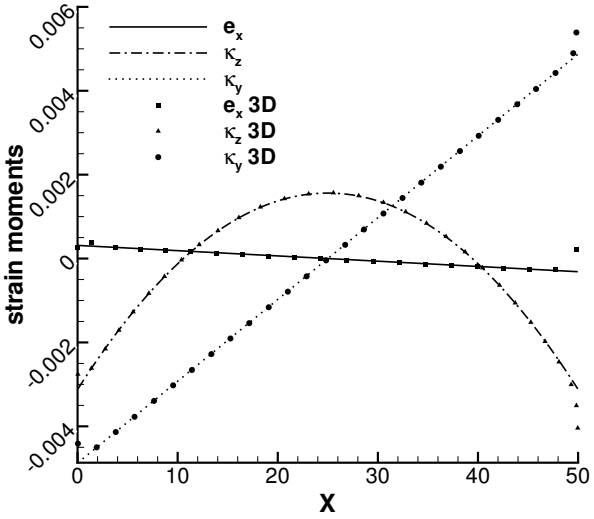

(a) Strain moments

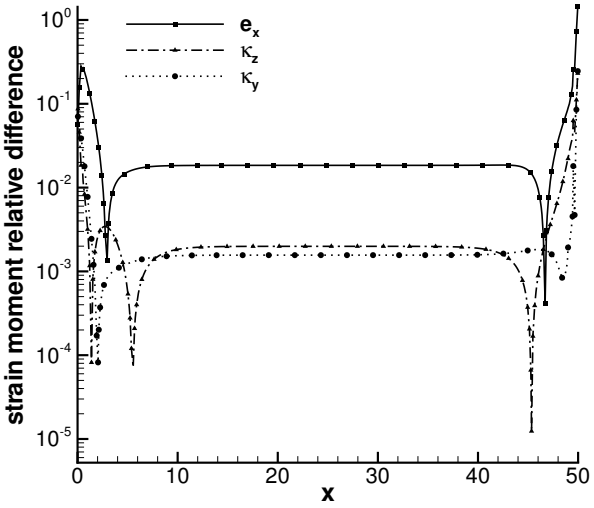

(b) Relative error

Figure 12: The first three components of the strain moments and the relative error between the beam theory prediction and the full three-dimensional calculations. The relative error is defined as $e_{\mathrm{rel}} = |e - e_{3\mathrm{D}}|/\max(|e_{3\mathrm{D}}|)$.

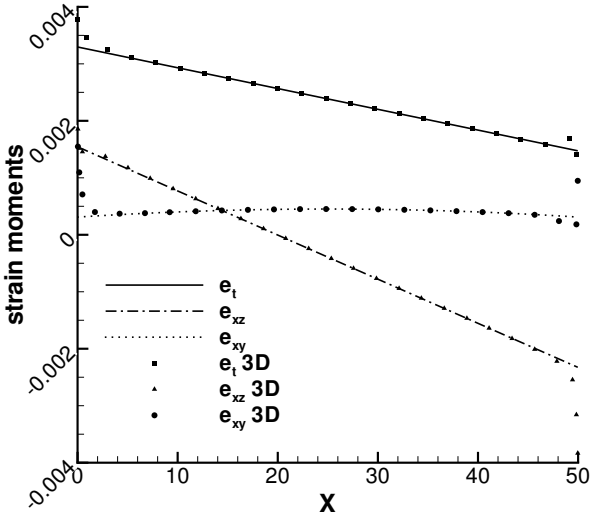

(a) Strain moments

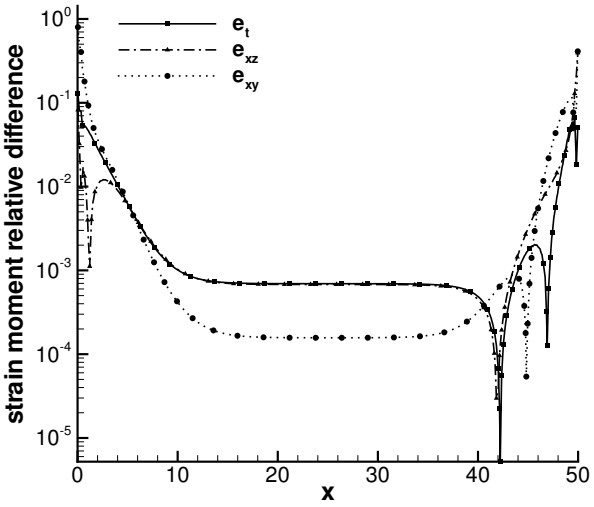

(b) Relative error

Figure 13: The last three components of the strain moments and the relative error between the beam theory prediction and the full three-dimensional calculations. The relative error is defined as $e_{\mathrm{rel}} = |e - e_{3\mathrm{D}}|/\max(|e_{3\mathrm{D}}|)$.

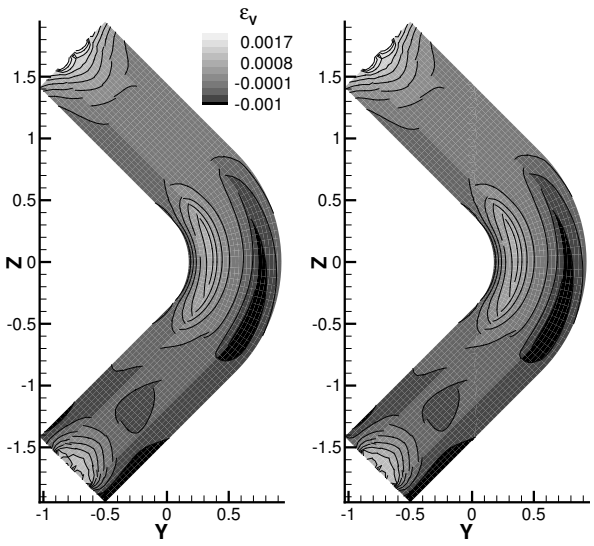

Figure 14: A comparison of the through-thickness volumetric strain $\epsilon_V = \epsilon_x + \epsilon_y + \epsilon_z$ at the cross-section $x = L/2$. The beam theory solution is shown on the left, while the full three-dimensional solution is shown on the right.

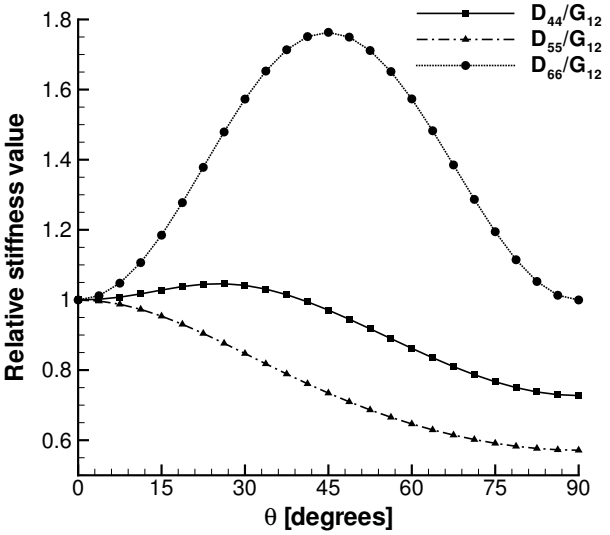

Figure 15: The variation of the diagonal components of the homogenized stiffness $\boldsymbol{D}$ representing the torsion, $\boldsymbol{D}_{44}$, and shear stiffnesses, $\boldsymbol{D}_{55}$ and $\boldsymbol{D}_{66}$, relative to the shear modulus G_{12}. The results are shown for the angle-ply beam over a range of ply angles from $\theta = 0^o$ to $\theta = 90^o$.

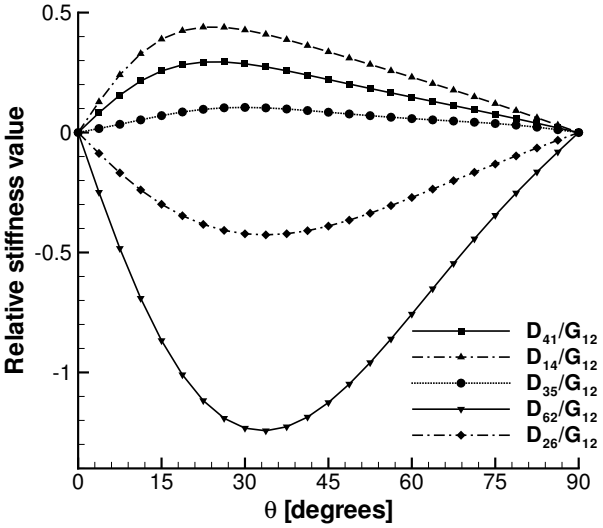

Figure 16: The variation of the off-diagonal components of the homogenized stiffness matrix $\boldsymbol{D}$ normalized by the shear modulus G_{12}. The results are shown for the angle-ply beam over a range of ply angles from $\theta = 0^o$ to $\theta = 90^o$.

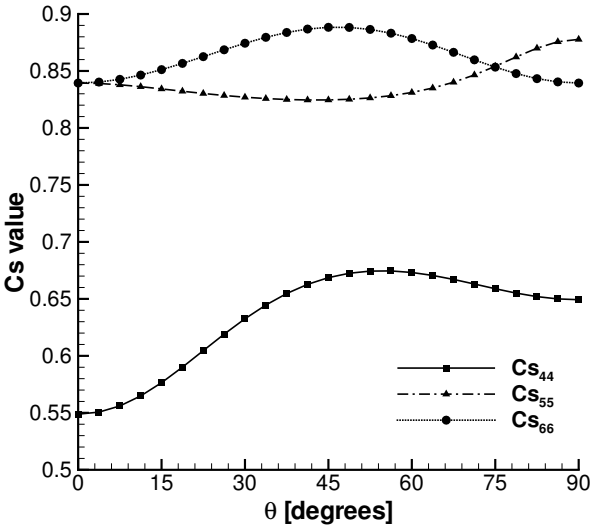

Figure 17: The variation of the diagonal components of the strain correction matrix $\boldsymbol{C}_s$ representing the torsion and shear strain corrections. The results are shown for the angle-ply beam over a range of ply angles from $\theta = 0^o$ to $\theta = 90^o$.

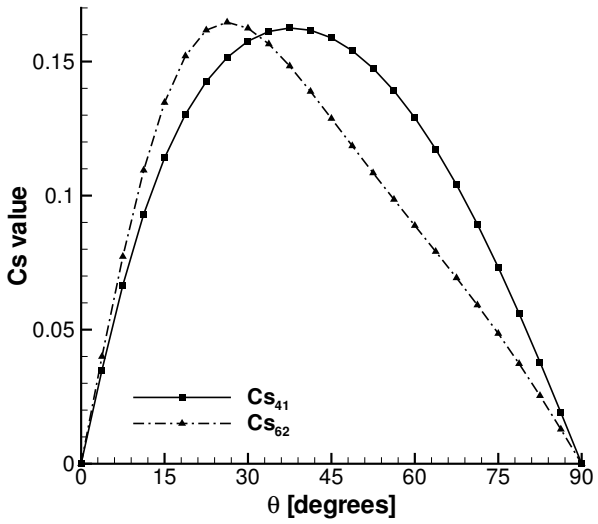

Figure 18: The variation of the off-diagonal components of the strain correction matrix $\boldsymbol{C}_s$. The results are shown for the angle-ply beam over a range of ply angles from $\theta = 0^o$ to $\theta = 90^o$.